Ore Genesis and Environmental Study of Pinpet Iron Deposit, southern Shan State, Myanmar

A dissertation submitted in partial fulfillment
of the requirements for the degree of
Doctor of Philosophy in Engineering

by

KYAW ZAY YA

Division of Sustainable Resources Engineering
Graduate School of Engineering, Hokkaido University, Japan

June 2020

Ore Genesis and Environmental Study of Pinpet Iron Deposit, southern Shan State, Myanmar

KYAW ZAY YA

Environmental Geology Laboratory
Graduate School of Engineering
Hokkaido University

ABSTRACT

Myanmar has great potential in a variety of metal and mineral resources, many of which have been poorly explored. The Pinpet deposit is the second-largest iron (Fe) deposit in Myanmar, located in the Shan Plateau, the eastern part of Myanmar. The probable ore reserve is estimated to be 10 million tons of hematite ore and 70 million tons of limonite ore, in which pilot-scale open-cut mining and beneficiation processes for low-grade ores started in 2003. However, the mine operations have been suspended since 2017, in part because of the possible contamination of heavy metals and hazardous elements into the surrounding aquatic environment and associated public concern. A scientific investigation of the source and degree of contamination in the stream near the deposit has not yet been conducted. Ore genesis in the Pinpet Fe deposit is not well understood, which also makes it difficult to assess the environmental risk because some Fe ore deposit types may contain a significant concentration of hazardous elements, such as arsenic (As) and uranium (U). Therefore, objectives of the dissertation are to reveal the ore-forming process based on geological survey and mineralogical and geochemical analyses of ores and host rocks and to understand the environmental impact by Pinpet iron mine's activities on the surface water qualities by quantifying heavy-metal and hazardous-elements concentrations of surface water and sediments in stream beds.

Chapter 1 provides the general background on Pinpet Fe deposit and its mining activity based on literature reviews, as well as the objectives of the dissertation. Chapter 2 focuses on the detail-geological mapping of the Pinpet deposit and the surrounding area. Based on the literature review, the study area is hosted by a lower Palaeozoic rock sequence (Silurian limestone), which is bounded by the NE-SW trend of major localized faults in which trends parallel to regional faults (Kyaukkyan and Htam Sang faults). The other minor cross faults (WNW-ESE trending) are also found in the middle part of the ore zone related to hematite ore zones. Field survey indicates that the well-bedded (trending 40° to 65°) hematite ore zone was controlled by WNW-ESE faulting while limonite ore zones showed poor bedding nature due to intensive weathered conditions. Hematite outcrops were also surrounded by magnetic anomaly caused by the presence of magnetite grains. However, Fe ore zones were constrained by country rock (limestone) with sharp contacts. Therefore, the results of the field survey suggest that the Fe enrichment in the overall ore zones occurred concordantly with sedimentation processes whereas mineralization of hematite ores was likely caused by later tectonic events.

Chapter 3 focuses on the mineralogical and geochemical characteristics of the Fe ores. Petrographic observation and whole-rock geochemical analysis indicate that the ores are primarily composed of hematite, goethite, magnetite, and other minerals including manganese oxides and barite. Arsenic was the most abundant trace element, containing up to 2 wt.%. However, sequential extraction results indicate that most (> 90%) of the As in the As-rich ore is hosted in insoluble fractions (e.g., crystalline Fe hydroxides and clay). Other trace elements such as copper (Cu), zinc (Zn), and U were not significantly enriched in the ores. Stable isotope analysis of Fe in the ores indicates the variable isotopic compositions, suggesting that Fe was precipitated from hydrothermal fluids in an open system. Fluid inclusion analysis of barite indicates that a low-temperature (~160 ºC) hydrothermal fluid and salinity ranging between 0.2 and 6.6 wt.% NaCl eq.

was responsible for the formation of barite. These results may suggest the hydrothermal fluid was formed by mixing of seawater with meteoric water.

Chapter 4 focuses on the geochemical characteristics of surface water and sediments in a stream flowing near the Pinpet deposit. The result of major dissolved element analyses shows that all the surface water samples were dominated by calcium (Ca^{2+}), magnesium (Mg^{2+}), and bicarbonate (HCO_3^-) ions, controlled by limestone bedrock in the study area. All the dissolved trace elements, including As, Cu, Zn, and Fe are in low concentrations, below the WHO standard as well as the proposed national drinking water quality standards in Myanmar. Bulk chemical compositions of the stream sediments indicate no significant past contamination by hazardous elements. Arsenic, Zn, and Cu concentrations in the sediments are similar to those in uncontaminated sediments, although some sediments in the tailings dam were probably transported to the middle reaches of the stream. However, arsenic in these sediments is mostly bounded in insoluble fractions.

Chapter 5 concludes the ore genesis model of the Pinpet Fe ore deposit and environmental risk associated with the development of the Pinpet mine. The sedimentary nature with bedding planes observed in hematite ore zones suggests that ores were formed during sedimentation processes. The Fe isotope data of the hematite and limonite ores suggest that Fe was precipitated by oxidative precipitation of ferrous iron from a low-temperature hydrothermal fluid in seawater. On the other hand, the spatial distribution of hematite ores and As-rich ores is along with the WNW-ESE trend, according to minor faults in the area, suggesting that mineralization of hematite ores and addition of As into the limonite ores occurred during later tectonic activities. Therefore, it is concluded that the Pinpet Fe deposit was formed as a result of multiple hydrothermal activities during both sedimentation and faulting events. Geochemical characteristics of surface waters and sediments in a stream flowing near the Pinpet deposit indicate that no significant past and present

contaminations of metals into the aquatic environments. Although As content in some ores were high, sequential extraction results indicate that most of the As in this As-rich ore is hosted in insoluble fractions, probably in the crystal structure of Fe hydroxides and clays. Therefore, As is unlikely to be released into the aquatic environment by interacting with water during future ore beneficiation processes should mining be re-established at Pinpet.

ACKNOWLEDGEMENTS

I'm deeply indebted to my supervisor, Dr. Tsubasa Otake, Associated Professor, Hokkaido University, Japan for accepting me as his student in Environmental Geology Laboratory, Division of Sustainable Resources Engineering, Hokkaido University. During my study period, he supported and guided me in my research both in field studies and laboratory experiments, which enable me to obtain hands-on experience in my study research. The patience and motivation he had for me helped me to successfully manage my daily life and school activities. Words not enough to express my sincere gratitude for all his generosity. I will be looking forward to more co-operation and working with him in the future. Much appreciation goes to Prof. Tsutomu Sato for his kind and valuable criticism and comments throughout my study. Not only did I get technical advice from him but also warm heartfelt kindness and support. The two professors undoubtedly helped me to achieve my research objectives and I will always remember and deeply thank them as I continue to progress in my career path.

My sincere appreciation to Dr. Ye Myint Swe, Deputy Minister, Ministry of Natural Resources and Environmental Conservation (former Director-General, Department of Geological Survey and Mineral Exploration, DGSE) and Directors, Deputy Directors from DGSE for nominating me for the Kizuna scholarship, KIZUNA program. Also, I would like to thank Dr. Thet Tin Nyunt (Director General, DGSE) for his encouragement and advice to conduct my research study.

I thank No. 2 Steel Mill (Pinpet) of the Ministry of Industry for permitting field surveys in the mining area and providing me the necessary data and information. During the field trip, much help was given to me by the mine geologists also thank DGSE geologists, Taunggyi branch office.

I sincerely appreciate Dr. Kenzo Sanemastu (Advanced Industrial Science and Technology, AIST) for accepting me to be part of his Mineral Resource Group for the internship course. He not only helped me in experiments but also during the field trips. I deeply appreciate his advice and research ideas in the fieldwork.

My sincere thanks to Saya Aung Kyaw Htun (Retired Lecturer, Geology Department, Yangon University) and Dr. Tun Naing Zaw (Associate Professor, Geology Department, Yangon University) for fieldwork and valuable discussions and their encouragements.

I also wish to thank the past and current lab mates of the Environmental Geology Laboratory, Hokkaido University who have contributed to my growth, for assistance during fieldwork, for their technical assistance in acquiring chemical data. I also learned a lot from my lab mates. I would like to say thank you all.

Finally, I wish to express my sincere appreciation to JICA for the scholarship during my study period at Hokkaido University, Japan. Besides, not forgetting all the JICA's officers and staff in Japan and Myanmar for all their support in field survey arrangements and others, needed logistics. I look forward to having a better future working collaboration with JICA for the benefit of Myanmar and Japan.

TABLE OF CONTENTS

Chapter 5: General Conclusions

LIST OF TABLES

LIST OF FIGURES

Chapter 1

Chapter 2

Chapter 3

Chapter 4

CHAPTER 1: General Introduction

1.1. Background

Myanmar has many types of mineral deposits such as tin-tungsten, antimony, lead-zinc-silver, nickel-copper-gold, iron-manganese as well as gem and industrial mineral deposits (e.g., barite, fluorite, gypsum, coal, etc.,). Despite Myanmar has the potential endowment, a large number of deposits have not been discovered and poorly explored due to decades of isolation, lack of funds, and technical know-how. The results are limited data on mineral resources and reserves and a lack of major exploration activity. Among the mineral deposits, the Pinpet deposit is one of the best-known iron deposits in Myanmar however limited research work.

Iron (Fe) ore deposit at Mt. Pinpet has been known since 1951 and exploration of the deposit was started in the year 1954. Initially, the stages of exploration were carried out by pitting and trenching, later followed by diamond drilling and geomagnetic survey. The drilling results indicated the ore body to have an irregular shape in the form of pockets. The first attempts to explore the mine were made in 1961 but stalled in 1962 after Burma's (Myanmar) first military coup. This was followed by geological work that was performed in 1982. A second attempt followed the 1991 cease-fire agreement. After that, the activities were stalled again, this time, however, due to the lack of funds. In 2004, Russia and the Italian company started to develop the Pinpet Fe deposit and to build up an ore processing plant. In 2006, the Russian state-owned company Tyazhpromexport ltd. announced to provide 150 million USD in equipment for the project. According to the Ministry of Industry (MOI), Myanmar, the iron processing mill (No.2 Pinpet Steel Mill) was to have a capacity to produce about 200,000 tons of pig iron annually.

The Pinpet Fe deposit is the second-largest known iron deposit in Myanmar. The deposit size is 4.02 km × 0.80 km × 90 m which consists of the estimated reserve of 10 million tons of

hematite (56.4 %Fe) and 70 million tons of limonite (42.6%Fe). Ore genesis in the Pinpet Fe deposit is not well understood. Previous unpublished reports (ESCAP, 1996) have classified the ore deposit variously as a limestone replacement, lateritic, or Fe-oxide-Cu-Au (IOCG) deposit. The ore bodies are composed solely of oxide ores: limonite ore (mainly goethite) and hematite ore. Limonite ores are particularly likely affected by lateralization. Arsenic contents in some ore zones are high, up to 0.25 % (Krupp-Rohstoff, 1962). Furthermore, about 30 million tons of limestone was observed surrounding of iron ore zone, that was used to make cement. The Pinpet mine has been mined by an open-pit method and the low-grade ores were undergoing the beneficiation process within the area. In 2017, the mine was temporarily suspended because of lack of economic viability and possible contamination of heavy metals and hazardous elements, such as Fe, arsenic (As), copper (Cu), and zinc (Zn) into the surrounding aquatic environments, due to public concerns about the effects of mining activities. On the other hand, in 2018 the Ministry of Natural Resources and Environmental Conservation (MoNREC) passed the much-anticipated Myanmar Mines Rules, repealing the previous mines rules passed in 1996. The Amendments Mine Law included the focus on environmental consideration, which was dependent on the type of permit applied. An investor was required to submit the Environmental Impact Assessment (EIA) and/or Environmental Management Plan (EMP) by the guidance of the MoNREC.

Mining and associated mineral processing and beneficiation have impacts on the environment. Unfortunately, this frequently led to serious consequences in Myanmar. The impact of mining depends on many factors, such as type of mining, the size of the operation, and the type of mineral deposit. Mining operations can adversely impact land degradations and hydrogeological conditions. Mining also has not only a social impact but also environmental impact on the surrounding area such as growing populations and metal contaminations which affects health conditions leading to high mortality rates. An environmental impact assessment is necessary prior

to the development of any new mine, indicating how environment management plans will deal with environmental issues during mine operations. The mine water and surrounding aquatic water quality are determined by the hydrogeological and geochemical characteristics of solid samples and water samples (surface water and groundwater). It is important that water quality is being monitored and recorded throughout the mine operation workings and also after closure so as to assess the potential environmental problems.

1.2. Location, climate, vegetation, and land use

The study area is situated at Pinpet range, Taunggyi Township, southern Shan State, Myanmar, about 11 km southeast of Taunggyi Township (Fig 1.1). The area is easily accessible by regular flight or road. The Pinpet mine is located ~3 km south of Nawng lang village. The study area is mountainous, located within the Pinpet range. This range comprises of five hillocks linking together. The highest point is 1382 meters above sea level and lies nearly in the middle of the ridge. The SW end of the ridge is narrow and long whilst the NE end is broad and short. Physio-graphically it has a conspicuous land feature, which can be divided into two portions such as lowland area and mountainous terrain. In general, the lowland area is found at the northern, eastern, and southeast parts of the study area as a rolling hill and flat plain. The mountain ranges of the southwest part are NE-SW trending and rugged and constitute several peaks, gorges and ravines, and complex geomorphic features.

The study area lies in a humid subtropical climate in which monsoon starts from June to the middle of November. The dry season is from March to the beginning of June. Annual rainfall is about an average of 1540 mm/yr. The lithology of the study area is covered by carbonated rock, usually present in very rugged terrain with steep slopes covered by fairly dense forest. In the siltstone and shale covered areas, the hill attains a moderate altitude and has fairly vegetative and

forest covers. Soil covered areas are good for cultivation and low-lying areas are cultivated for rice, crop, corn, tea plant, peanut, and vegetable garden. The study area includes not only the mine area (Pinpet Fe ore zone) but also cultivated areas in the eastern part of the ore zone. The Nan-tank-pauk stream pass-through from north to south in the eastern part (Hopong valley). The stream water has been used not only for mineral processing (beneficiation), including washing and magnetic separation but also in agricultural activities and human needs (e.g., laundry). The farmlands have been developed mainly along the Nan-tank-pauk stream and cultivated by using traditional methods, which utilize available natural resources (such as animal waste) combined with a synthetic chemical such as fertilizers and pesticides (Cho Cho Myint, 1989). Small villages, in which populations are ~7,000 people in total, are also located along the Nan-tank-pauk stream. Most villagers who are farmers and breeders living near Mt.Pinpet are of the Pa'O ethnic group with Shans and Indians people also living in the area.

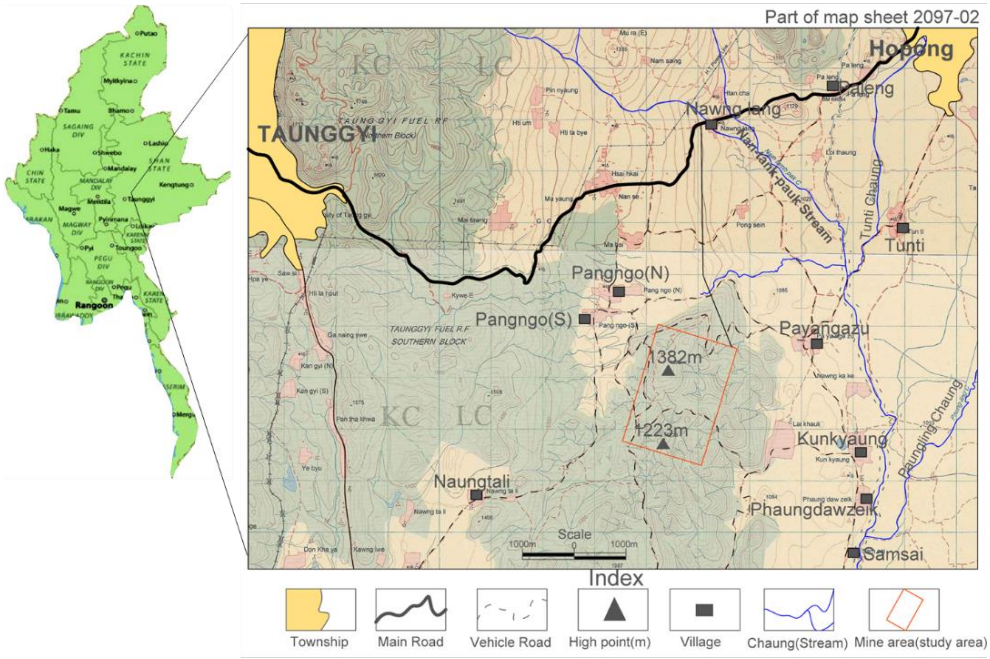

Fig 1.1. Location map of the study area in Taunggyi and Hopong township (modified after DGSE, 2015).

1.3. Previous works

The previous studies conducted in the area are limited mostly due to restrictions of access to the area by military base company, Myanmar Economic Corporation (MEC). A few studies include Griffith (1995), which reported the characteristics of Pinpet iron deposit. The author reported the characteristics of ore in terms of metallurgical aspects, such as silica to alumina ratio which affects smelting processes. The ratio was found very high and recommended more assessments of the deposit. Savanholm (1955) reported on Fe ore deposit exploration in the Taunggyi area, with a view of conducting extensive geomagnetic reconnaissance surveys to locate potential areas for Fe ore deposits. However, no detailed geological and mineralogical survey, nor ore genetic study has been conducted. Nodth (1956) reported on the inspection of the drilling results of the Pinpet ore deposit. The depth of the sampled drill hole was 90 meters and did not reach the base of the ore zone. It was apparent that the sampled drill sections contained yellow to whitish sandy clay of varying thickness. The Fe content of ore was up to 20 wt% Fe in the sandy clay. Occasionally, interposed sandy clayish rocks were high Fe content. The author suggested that the Pinpet deposit can be classified into a lateritic weathering type regardless that no petrological or mineralogical analysis was conducted. The author's aims were focused on mine design and estimation of ore reserves of Pinpet deposit. Srivastava (1956) conducted some geological investigations, exploration, and development of the Pinpet iron ore deposit. However, discussion for the origin of the Fe ore deposit could not be concluded but layered character observed in the exploratory cuts and pits. Nayudu (1955) reported the origin to be limestone replacements based on his observation of siderite ($FeCO_3$) in the limestone. However, Srivastava (1956) did not observe siderite through optical analyses also chemical analyses of limestone samples did not indicate any occurrences of ferrous carbonate. He suggested that more than one

factor was involved in the formation of the deposit, though no microscopic study was conducted on any ferrous carbonate host rocks.

Krupp Rohstoffe (1962) performed preliminary exploration studies on the Fe ore deposit based on a topographic survey, trench, and pitting survey including other surface and subsurface data. Some preliminary results indicated possible ore reserve in hematite and limonite ores as well as a concentration of uranium (U). Borehole data showed black shale was the host for U mineralization. However, the study did not suggest the ore genesis of the Pinpet iron ore deposit. Bender (1997) mentioned the Pinpet iron deposit is of IOCG type, and other geologists considered that the Pinpet Fe ore zone was formed by contact metamorphism by the intrusion of igneous rock, therefore classified as a skarn type. Ahtar Hlaing with the DGSE team (2015) worked for Fe exploration in the Pinpet extension area. This report [in Myanmar language] focused on the estimate of Fe ore tonnage in the extension area. They could not also reach a conclusion for the genetic type of the deposit.

1.4. Objectives of this study

The main objectives of this study are to (1) understand the ore formation processes and construct the ore deposit model of the Pinpet Fe ore deposit based on the geological surveys, mineralogical and geochemical analyses of ores and host rocks, and (2) investigate the geochemical characteristics of surface waters and sediments in stream beds with a view to understanding the water qualities and heavy-metal and hazardous-elements concentrations by the mining activities.

1.5. Dissertation structure

This dissertation is divided into five chapters:

Chapter 1 briefly explains the history of the study area of Pinpet Fe deposit and literature reviews. This chapter includes the objective of the study also lays out the framework of this dissertation.

Chapter 2 explains the regional geology and structural geology of the study area based on the literature reviews including works by the Department of Geological Survey and Mineral Exploration (DGSE) as well as my detailed geological mapping on the main ore zone to delineate the nature of the Pinpet Fe deposit.

Chapter 3 investigates the mineralogical and geochemical characteristics of Fe ores and host rocks to understand the ore-forming process. Furthermore, stable isotope and fluid inclusions studies were conducted to obtain hydrothermal fluids involved in the formation of the ores. Additionally, trace elements (such as arsenic, copper, zinc, and uranium) concentrations in the ores with acid-digestion as well as sequential extraction were analyzed to examine their concentration and speciation in the Fe ores.

Chapter 4 investigates the geochemical characteristics of surface water and sediments in the stream flowing near the ore zone for environmental risk assessment by mining activities. Part of this chapter was included in a published paper as Zay Ya, K., Otake, T., Koide, A., Sanematsu, K., Sato, T. (2020) Geochemical characteristics of ores and surface waters for environmental risk assessment in the Pinpet iron deposit, southern Shan State, Myanmar from *Resource Geology* (http://doi.org/10.1111/rge.12231).

Chapter 5 concludes the ore genesis model of the Pinpet Fe ore deposit based on field survey, the mineralogical and geochemical characteristics of Fe ores and host rocks, and furthermore, the environmental risk associated with the development of Pinpet mine.

CHAPTER 2: Geological mapping of Pinpet deposit

2.1. Introduction

Geological mapping is the process of selecting an area of interest and identifying all the geological aspects with the purpose of summarizing the geological reports. The geological map includes the distribution of various rock types, the structures, geological formations, distribution of ore deposits, and fossils. The quality of a geological map will depend upon the accuracy and the precision of the fieldwork. Furthermore, the quality depends on the completeness with which certain data, both geologic and geographic are present on the map, and on the care with which scale, color, conventions, etc. are chosen to the best results (Eckel, 1902). We used four-time enlargements of 1:50000 UTM map sheet no 2019-02 and aerial photographs, land-sat (satellite) image in the field to obtain geological features, geological information (such as lithologic units, sample location points, outcrop nature), and outcrop mapping. A systematic geologic outcrop mapping was performed in the field and all available geological information was recorded.

2.1.1. Regional geology of southern Shan State

The Shan Plateau in eastern Myanmar consists of Cambrian-Ordovician sedimentary sequences with localized Ordovician volcanic rocks and volcaniclastics (Aye Ko Aung, 2012) unconformably overlain by thick Middle-Upper Permian limestone sequences. The study area is in Shan-Thai Block (Eastern Highland/Shan Plateau) with an elevation of more than 1,000 meters above sea level (Fig 2.1). Eastern Highlands Province of Shan Plateau is composed of a crystalline basement and a weakly metamorphosed turbidite sequence of probable Late Precambrian-Early Cambrian age, overlain by a thick sequence of Palaeozoic-Mesozoic continental shelf (Aye Ko Aung and Cocks 2017; Zaw Win *et al*., 2017). Thick Ordovician limestone and siltstone deposited under littoral and shelf conditions are found in northern and southern Shan State together with

strata-bound carbonate-hosted lead (Pb) - zinc (Zn) deposits (e.g., Bawsaing), barite deposits (e.g., Ani-sakan and Kyaukup), and Fe deposits (e.g., Kyatwingye, possibly younger age). Silurian phacoidal (lenticularly deformed) limestones and clastic, as well as local tuff and ash beds in southern Shan State, are associated with antimony deposits (e.g., Loi-Har-Myar), manganese (Mn) deposits (e.g., Hwe-tak), and Fe deposits (e.g., Pinpet).

The regional geological map of Taunggyi is shown in Fig 2.2. In the east of the study area, lower Paleozoic rocks are exposed such as Ordovician rocks of Lokepyin formation, Wunbye formation, Nan on formation, Silurian rocks of Linwe formation, Wabya formation, Carboniferous age of shale, pebbly schist, sand-shale intercalation limestone, and Plateau limestone Group of Nwabangyi Dolomite formation and Thitsipin limestone formation The western and northern parts comprise of exposed Ordovician, Silurian, Permian to Triassic age carbonate rock sequence. These carbonate sequences are a large anticline plunging to the south. The Nwabangyi dolomite formation is well exposed in Taunggyi- Hopong road section. In the east of the study area, Hopong plain is remarkably a low-lying area. This plain is trending N-S and extending to the south. West of the study area has a remarkable Heho plain and Pintaya range composed of Ordovician, Silurian, Devonian, and Permian ages rock sequences. Fe ore deposits are observed (Mt. Pinpet) and in the northern part of the study area including manganese ore deposits which occur in Paleozoic units.

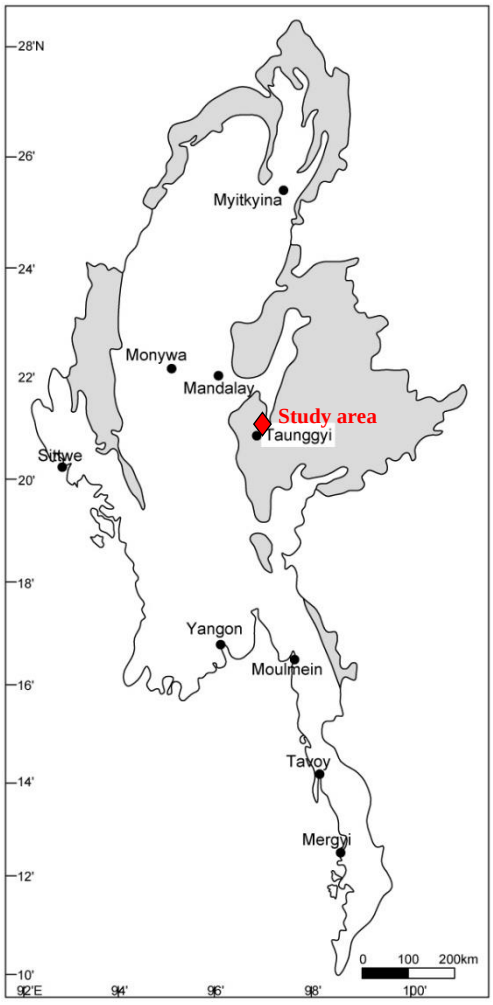

Fig 2.1. Map showing physiography of Myanmar. Light grey color denotes land above 1000m (from Barber et al., 2017).

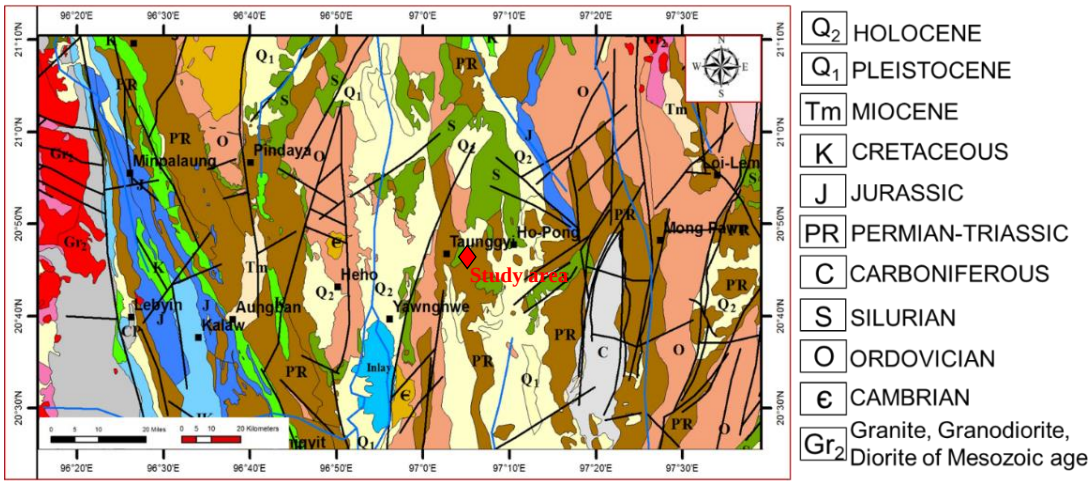

Fig 2.2. Regional Geological Map of Taunggyi Area (DGSE, 2015).

2.1.2. Structural geology of southern Shan State

Myanmar can be subdivided into four main tectonic provinces namely from west to east Rakhine Coastal, Western Ranges, Central Myanmar Basin, Eastern Highland (Shan-Thai Block). Eastern Highland, including the Shan Plateau, forms part of the Sibumasu (Sino- or Siam-Burma-Malaysia-Sumatra) Block, which extends southwest from Yunnan through Myanmar to Thailand, the Malay Peninsula and Sumatra (Metcalfe, 1996). The west margin of Sibumasu is a linear north-south belt between the dextral strike-slip Sagaing Fault and the Shan Plateau, known as the Shan scarps. Maung Thein (1973) described a concise work on tectonic features of Myanmar that are approximately in the north-south trend, following the general orientation of the Himalayan-Indonesian orogeny, which is an eastern segment of the Alpine-Himalayan Orogenic Belt. The Eastern Highlands include the eastern frontier ranges of Kachin State, the Shan Plateau in the middle, and the Tanintharyi Ranges and the Myeik shelf in the south. The Eastern Highlands and Central Myanmar Basin are divided by Shan Scarp Fault. Tectonically, the study area is situated in the western part of the Sibumasu Terrane (Metcalfe, 2009; 2011). During the Early Permian, the Sibumasu Terrance rifted and separated from eastern Gondwana, and drifted northward from southern to northern hemispheres (Metcalfe, 2009). At the beginning of the early Middle Permian, marine sedimentation was initiated as a widespread carbonate platform in the western Shan Plateau region, developing into a warm, open, shallow shelf sea (Zaw Win *et al*., 2017). The physiography is largely controlled by faults in nearly all directions.

Surrounding of the study area are the two major regional faults, such as Kyaukkyan fault and Htam-Sang fault. They are general trends from north to south direction. Kyaukkyan fault is one of the prominent seismotectonic features (Win Swe & Win Naing 2008; Soe Min *et al*., 2016). It is extending in the nearly north-south direction and small lineament, branching of cross fault in E-W direction. The two parallel faults roughly trend NE-SW direction and fault scarps

sporadically occur along the fault valley (Hopong valley) (Fig 2.3). This structure appears to be largely important in controlling the Pinpet Fe ore zone since the mineralized zone occurs between the two faults and may have been considered as an elevated fault block. WNW-ESE trending diagonal minor faults are also found in the mineralized shear zone associated with hematite ore zones.

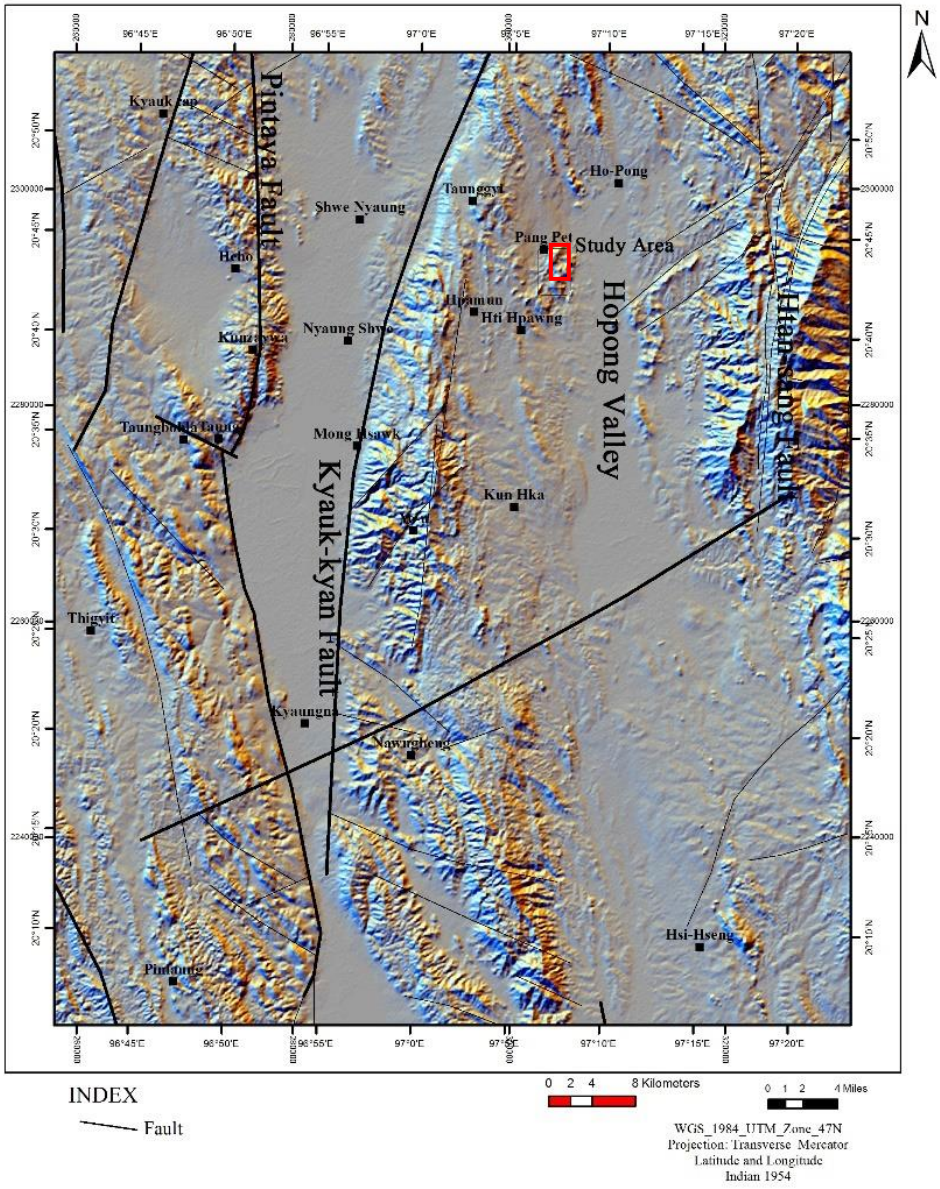

Fig 2.3. False-color satellite image of Taunggyi-Hopong area, southern Shan State (DGSE, 2015).

2.1.3. Previous mapping of Pinpet extension area by DGSE

In 2015, the DGSE team worked on the construction of geological mapping in the extension area of the Pinpet Fe deposit (Fig 2.4). According to the report, major parallel fault systems (NE-SW direction) and minor cross fault trending (NNW-SSE direction) controlled the extension iron zone comprising of hematite and limonite ores. Geophysical measurements (magnetic, resistivity) revealed that the hematite ore zone was covered by a weathered limonite zone. The vertical electrical sounding (VES) method showed a thickness of the Fe zone is 60 meters and overlie on the carbonate bedrock in the deeper portion. In the periphery of the extension ore zone, phacoidal limestone and brecciated dolomitic limestone were observed. The high-grade iron ore zones were scattered bounded by clay outcrop with limonite ores. The geochemical analyses showed that the average grade of hematite ores is 56.3 Fe wt.%. The drilling result in the upper part showed the reddish color clay with iron fragments zone and then hematite zone with a minor amount of limonite ores. Some of these Fe ores were hosted by clay layers (Figs 2.5, 2.6). Some drill holes did not intercept the iron zone because silty clay was covered in the upper position (Fig 2.6). However, the extension area of iron ore zones existed on the limestone unit (Figs 2.5, 2.7). In the extension area, hematite ore is abundant than limonite ore. According to the geophysical survey and subsurface survey, the report indicated that the extension area of the Pinpet ore zone was likely a residual Fe deposit. Comparing with the previous geological map and extension ore zone area, they suggested that the main ore zone of the Pinpet mine area and extension area of rocks sequences are similar lithologic units as shown in Table. 2.1.

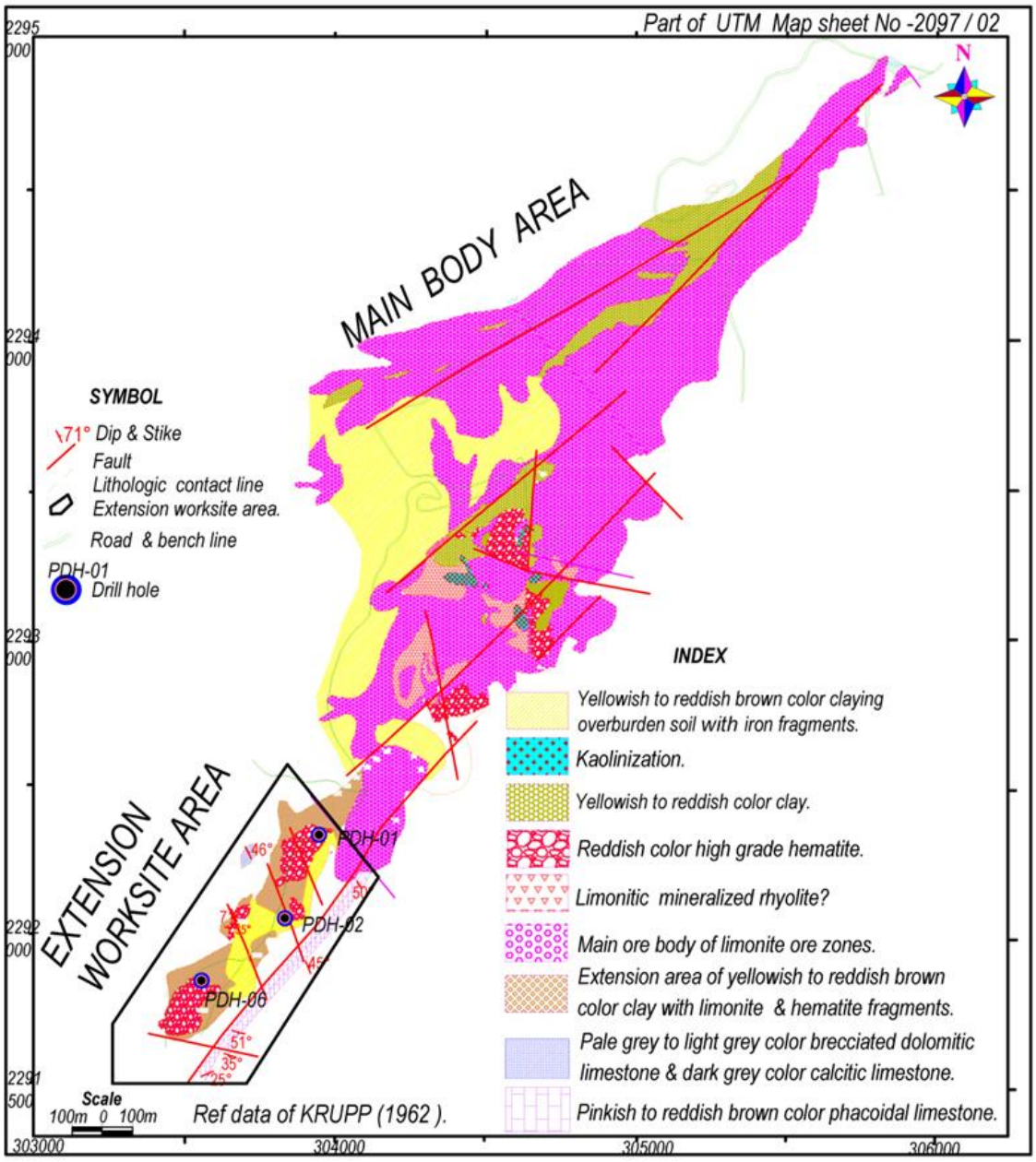

Fig 2.4. Map showing the main ore body and extension iron ore zone of the Pinpet area (DGSE, 2015).

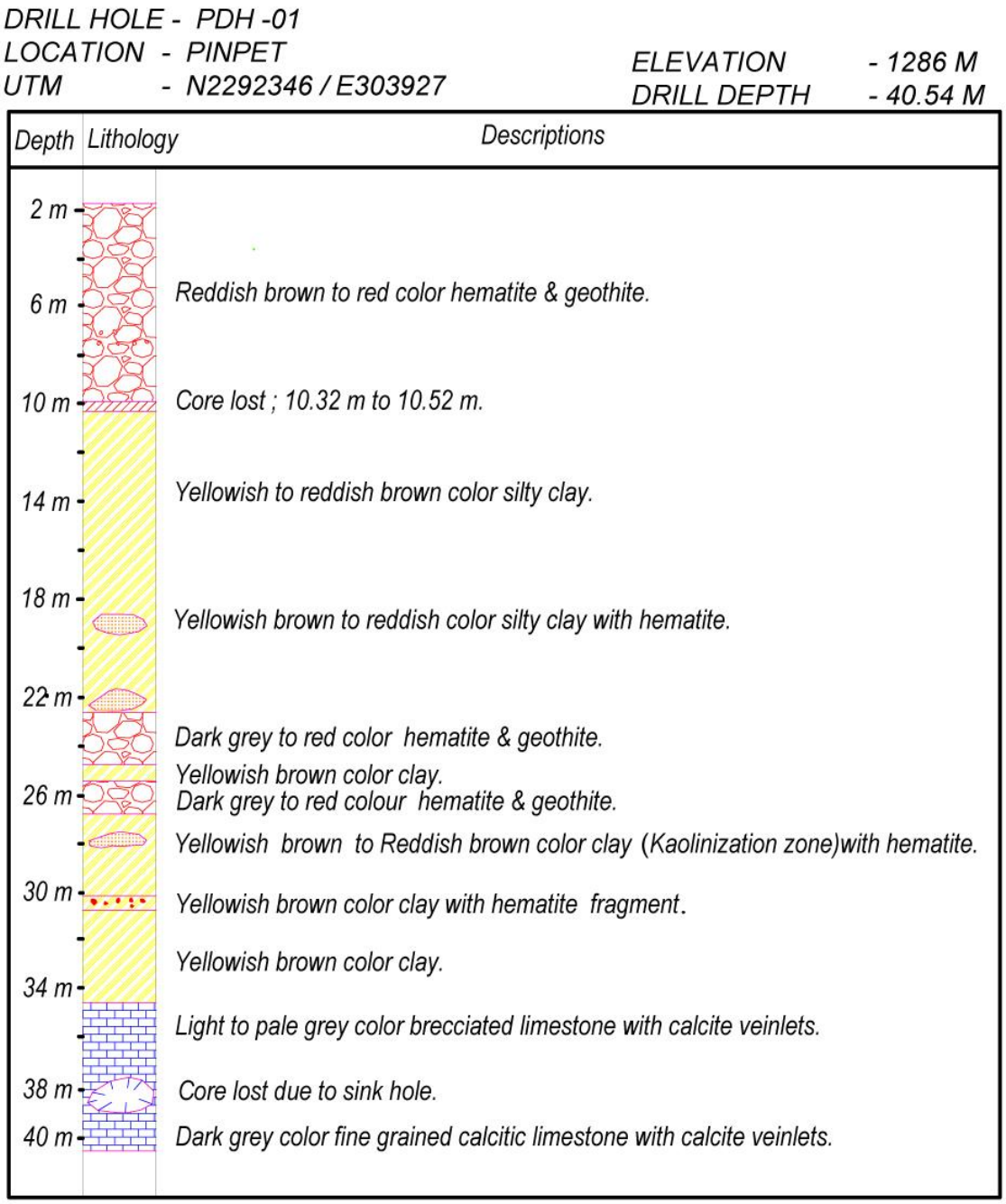

Fig 2.5. Vertical profile of drill hole no-01 in the extension ore zone of Pinpet deposit (Source from DGSE, 2015).

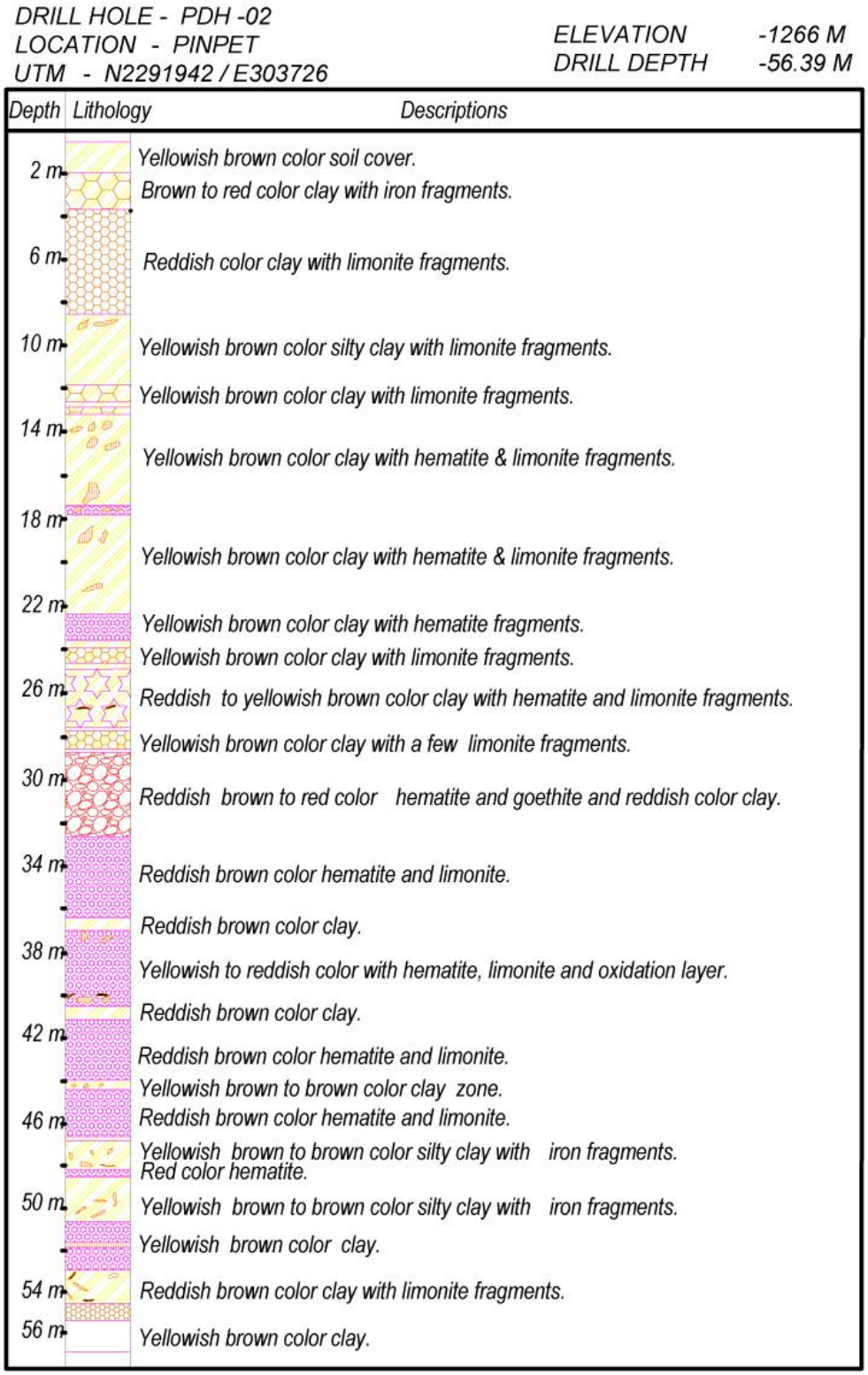

Fig 2.6. Vertical profile of drill hole no-02 in the extension ore zone of Pinpet deposit (Source from DGSE, 2015).

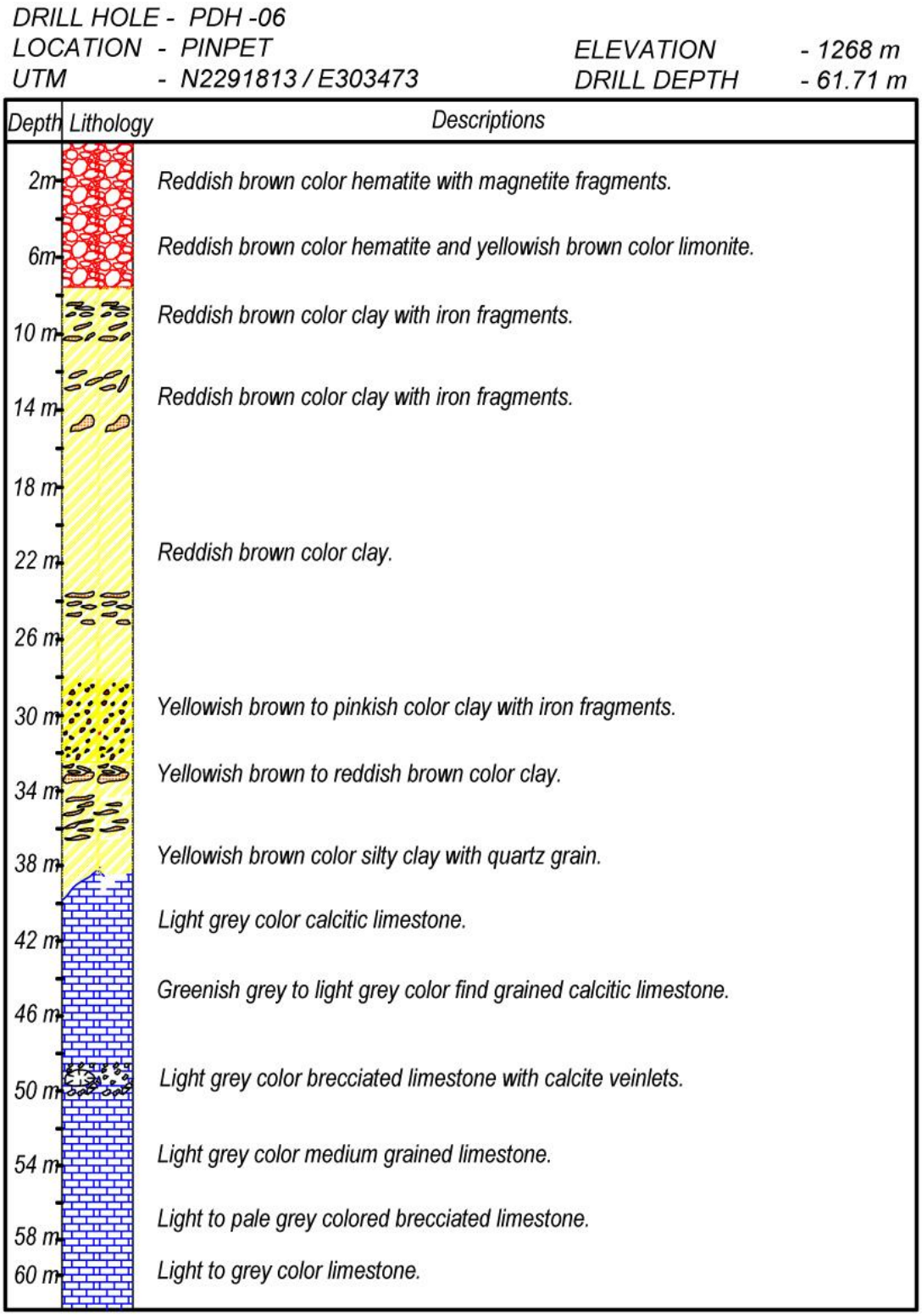

Fig 2.7. Vertical profile of drill hole no-06 in the extension ore zone of Pinpet deposit (Source from DGSE, 2015).

Table 2.1 The stratigraphic units of the surrounding of Pinpet iron ore zone area.

Geological age	Stratigraphic Unit	Lithologic description
Early Quaternary	Older Alluvium	Yellowish to reddish color soil cover
~~	Unconformity	~~~~
Early Triassic to Late Permian	Nwabangyi Dolomite Formation	Light grey to dark grey color highly brecciated dolomitic limestone
Early Permian	Thitsipin Limestone Formation	Pale grey to dark grey color massive limestone
~~	Unconformity	~~~~
Early Silurian	Linwe Formation	Reddish to yellowish color Phacoidal Limestone and shale

2.1.4. Objective of detailed mapping in this study

The objective of detail mapping was to get as much information on the relationship of ore zone and country-rock types, style of mineralization, the structural character of the bedrock, physical characteristics, such as color and texture and to better understand the distribution and thickness of overburden. A detailed geologic outcrop mapping and sampling were performed during field works (April to May-2018) and all available geological information was recorded (such as host rocks unit, iron zones). Collecting of representative rock and ore samples were carried out at the localities where lithologic units are well exposed due to erosion, folding, and faulting.

2.2. The result of mapping

Limonite ore zones are a major portion of the deposit showing weathering characteristics on the surface throughout the entire length of the hill and almost limonite outcrops are poorly bedded (2.8a). The weathered limonite outcrop located in the central part of the ore zone has a magnetic portion with magnetite grains that attracts the hand magnet (Fig 2.8b). Limonite outcrop showed a porous and cavernous structure, and iron rose structure (Fig 2.8c, d) and the botryoidal nature of secondary iron ores were observed in the cavities on the limonite surface (Fig 2.8e, f).

Two types of hematite were observed, earthy type and compact type, compact hematite without any admixture minerals which can be observed with the naked eye although slightly magnetic. The hematite ore zone was observed in the middle portion of the Fe ore zone with well-bedded nature which trending is 40°~ 65° (Fig 2.9a). Some outcrops showed the shearing effect which has given rise to cleavage planes as indicated by the presence of polished surfaces and slickensides on the surface (Fig 2.9b, c). Generally, uppermost 1 to 1.5 meters are slightly weathered and the disintegrates into small first to pea-size pieces which are embedded in an earthy hematite matrix, which has given rise to cleavage planes and breaking the whole mass into small rhombohedron (Fig 2.9d, e). Earthy type is loose, coarse to fine-grained, occurring below the weathered zone of limonite zones and limonitic clay zone. The banding or layer growth nature of hematite was observed in the compact hematite zone (Fig 2.9f).

The iron ore zone was a lenticular shape, existing at the highest elevation of the surrounding hill, and orientation was NE-SW direction. The Fe ore zone was dissected by numerous faults striking which are the major faults, parallel to regional faults (NE-SW direction), and minor cross faults (WNW-ESE direction). A series of the parallel fault and their related cross fault exists in the study area. The ore zones and carbonate rock (e.g. Permian limestone) uplifted by the regional faults relative to the major parallel faults (Fig 2.10a). The lower level of the ore

zone was observed limonitic boulder and floats with clay outcrop (2.10b). The western part of the iron-zone was well-bedded reddish to pink color phacoidal limestone which trend is 340º and with west-dipping. However, east-dipping appeared in the eastern part of the ore zone. The periphery of the ore-zone included limonite outcrop however the central part of the ore zone has hematite outcrop, magnetic anomaly outcrop, poor bedding nature of phacoidal limestone, and reddish color clay outcrop. The Fe ore zones were constrained by the country rocks (limestone) with sharp contacts (Fig 2.11), which correspond with the shape of the ridge aligned to the host rock (limestone) bedding. However, host rock (limestone) showed anticline and syncline nature.

Fig 2.8. Photograph showing a poor bedded nature of limonitic outcrop (a), magnetite grain in weathered limonite outcrop (b), cavernous structure of limonitic ores (c), yellowish-brown colored iron rose texture of limonite ore (d), botryoidal nature of limonite ores (e, f).

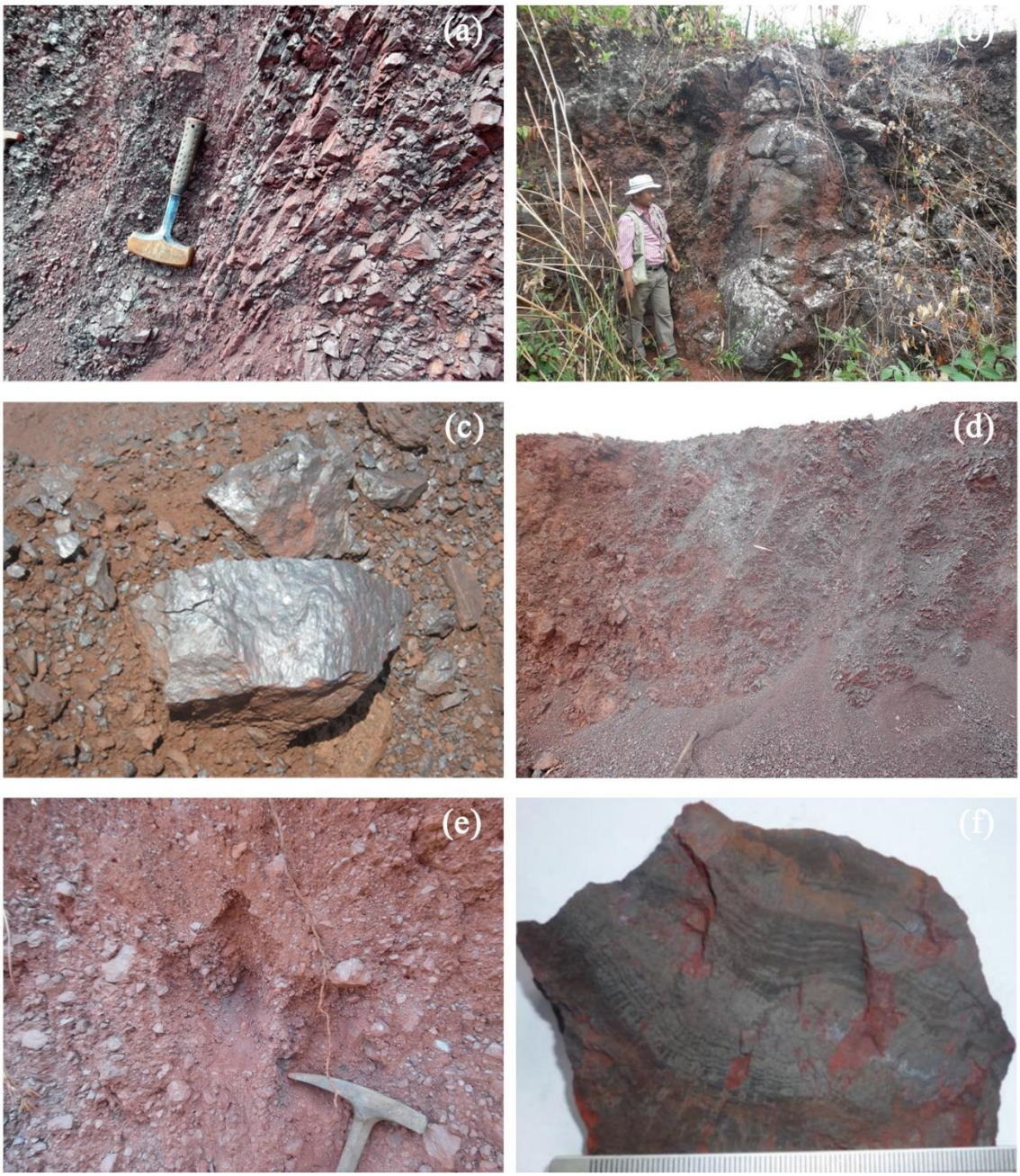

Fig 2.9. Photographs showing of well-bedded nature of hematite ore zone (a), evidence of the shearing effect on hematite outcrop (b), the polished surface character of hematite ore (c), the pea-size rhombohedron hematite grains (d, e), growth texture in hematite ore (f).

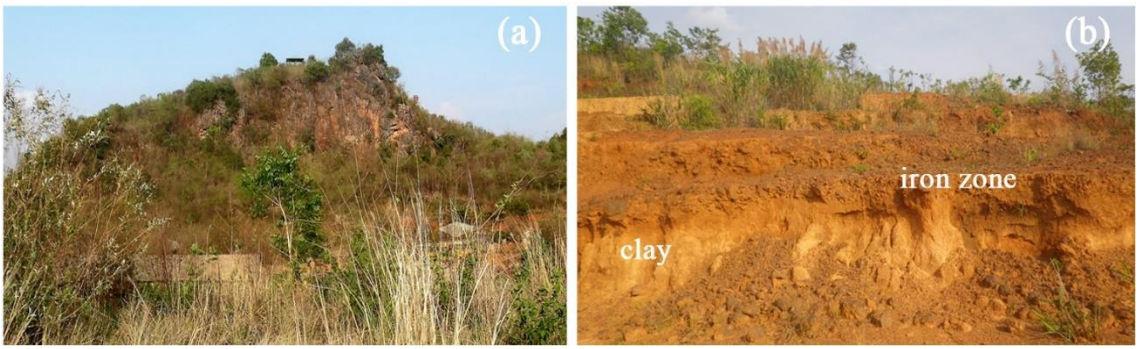

Fig 2.10. Photograph showing the fault trend on Thitsipin Limestone Formation (a) and clay outcrop with overlay limonitic iron zone (b).

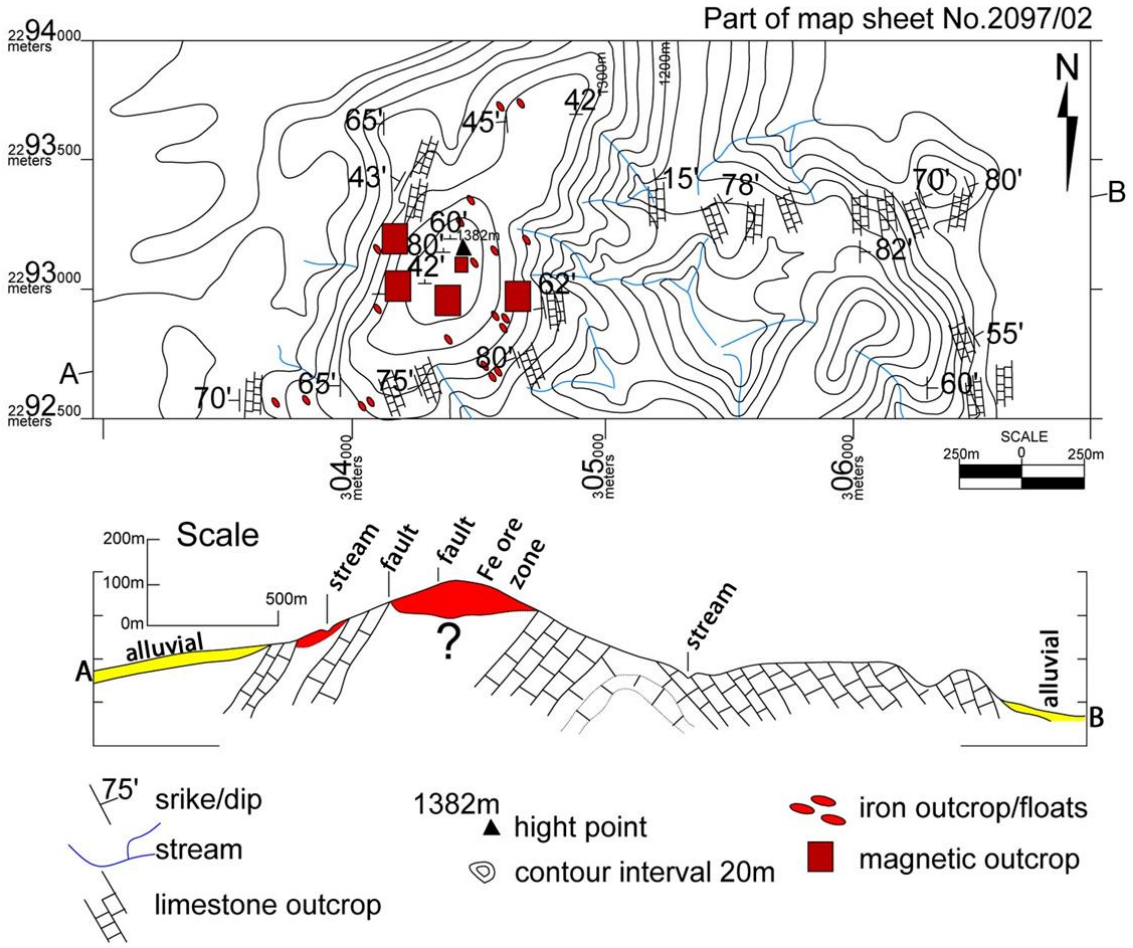

Fig 2.11. Detail outcrop mapping and cross-section along with A to B.

The study area is mainly composed of three (3) geological formations namely: the Nwabangyi dolomite, Thitsipin limestone, and Linwe Formation. The periphery of ore zones was covered by yellowish to reddish color soil. The following lithostratigraphic units are well exposed in the study area shown in Table. 2.1. The study area (Pinpet iron deposit) has hosted in two kinds of major host rocks, such as the Silurian age of limestone and shale/clay rocks.

Linwe Formation included purple to grey colored phacoidal nature limestone, ferruginous mudstones, siltstone, and shale was exposed at the periphery of the ore body and exposed in the southern part of the study area. The limestone outcrops are mostly medium to thick-bedded, medium-grained with a phacoidal texture, and minor fold characteristics were observed (Fig 2.12a). The Linwe Formation limestone was easily noted in the study area due to its texture. The limestone and Fe ore zone of the Linwe Formation were displayed sharp contacts (Fig 2.12b) in the western part of the ore zone. The soft and thin-bedded reddish to purple colored and yellowish colored shale outcrop was observed in the study area. The nature of the outcrop is highly jointed, fine to medium grain, and poorly cemented (Fig 2.12c). The periphery of the ore body has yellowish color clay outcrops especially exposed in the northern and southern part of the iron ore zone. However, a highly altered buff to pink color clay outcrop was observed in the middle part of the study area, near the hematite outcrops (Fig 2.12d).

Thitsipin Limestone Formation comprised pale grey, grey, and bluish-grey colored, micritic to fine-grained limestone and a lesser amount of dolomitic nature limestone was shatter pattern is also present. It is commonly massive but locally thick to medium-bedded, hard, and compact rock. The grey to bluish-grey colored, medium bedded. This unit is mainly exposed in the east and southwest part of the study area and trends nearly NE-SW direction. Some outcrops are show folding and fragile nature (Fig 2.13a, b) was observed in the study area.

Nwabangyi Dolomite Formation mainly exposed in the northwest part of the study area and along the Taunggyi-Hopong car road. The formation is composed of light grey to dark grey colored, fine-grained, highly brecciated, dolomite with a shattered pattern shown in Fig 2.13c.

The western part of the study area was observed the barite outcrop which trend is NS direction and 65º West dipping (Fig 2.13d). The barite outcrop located in the weathered iron zone.

Fig 2.12. Photograph showing the minor fold characteristics of phacoidal limestone (a), sharp contact of limestone outcrop, and an iron-zone (b), highly jointed clay outcrop (c), yellowish-brown to reddish color highly altered clay outcrop (f).

Fig 2.13. Photograph showing of grey colored medium to thick-bedded Thitsipin Limestone (a, b), grey-colored brecciated Nwabangyi Dolomite (c), barite outcrop (d).

2.3. Discussion

2.3.1. Stratigraphic control of mineralized ore zone

Localization of mineral deposits is controlled by geological conditions in the area such as the stratigraphy of host rocks, lithology, and geological structures such as folding, faulting, and igneous intrusions which determine the mineralization of the region. Rock successions formed under the marine basin and continental margins are the sites for deposition of sedimentary type deposit (Ram Bahadur and Kabi Raj Paudyal, 2019). According to the distribution pattern and shape of the rock units, the Pinpet area was considered as a large NE-SW trending anticline with outcrops of Silurian age limestone in its core. This formation is formed as an anticline with the

NE-SW axial plane and plunging to the north. The shape of the deposit is corresponding to the shape of the ridge and alignment to the host rocks' bedding. During the sedimentation period, the ferruginous sediments were deposited above the carbonate sequences mixing with clay rocks (Figs 2.5, 2.6, 2.7). The Fe ore zone was hosted in a carbonate sequence of the Silurian age with sharp contacts (Fig 2.11). The northern and southernmost part of the ore body pinches-out and narrow than in the middle part of the ore zone (Fig 2.4). The sequence of rocks, the Linwe formation, represents the most favorable carriers of ore. In the middle part of the ore-zone, the relationship of bedding cleavages and iron ore are unclear due to the poor nature of the outcrop. But periphery of ore zones was constrained by carbonate rock sequence, hence, stratigraphic control is one of the processes that govern the formation of the Pinpet Fe ore zone.

2.3.2. Structure control of mineralized ore zone

The structure is arguably one of the principal controls of mineralization. It leads to the formation of high fracture shear zones which provide pathways of the enhanced permeability and fluid flow during syn or post mineralization. In the study area, two kinds of faults direction can be classified. The first one is NE-SW direction major parallel faults, which are related to cross fault. The two regional fault relative major parallel faults uplifted the ore zones and carbonate rock (e.g. Permian limestone) as shown in Fig 2.10a. These parallel major faults systems have coincided with the regional tectonic fault trend, i.e. Kyauk-kyan Fault and Htam Sang Fault (NE-SW direction).

The Fe ore zones were found between two major parallel faults (NE-SW) direction. Furthermore, faults pass through the ore zone along with the sharp contact of Linwe Formation. The Fe ore zone represented by hematite and limonite mineralization is bound by two parallel faults system in the carbonate rock sequences (Fig 2.4). The second one is the diagonal fault trend,

WNW-ESE direction of minor faults. The major parallel faults and minor cross faults encountered in the middle part of the ore zone. As a result of the appeared mineralization of hematite ores. Tectonic movements were evidenced on the hematite outcrop surface (Fig 2.9b). The Fe ore zone might be uplifted by the structures as well as hematite ore zone was caused by later diagonal cross faults.

2.4. Conclusions

The Fe ore zone was composed of limonite and hematite ores which are situated along the entire length of the hill, corresponding to the shape of the ridge. The Fe ore zone was dissected by numerous faults striking which are the major faults, parallel to regional faults (NE-SW direction), and minor cross faults (WNW-ESE direction). The lower elevation was observed boulder and pebble sizes limonite ores. Limonite ore is a major portion of the deposit occupies about 70% of the area with poor bedded nature due to weathered condition. Although, magnetic anomaly could be observed in the middle part of the ore zone due to the presence of magnetite grains. The barite outcrop (trending 350º/65º W) was observed in the weathered limonite zone. Limonite ores were observed to be botryoidal in nature in the cavities, porous, and cavernous structure suggesting the secondary origin due to weathering processes. A well-bedded hematite ore zone was observed in the middle part of the ore zone which was related to minor cross faults (WNW-ESE rend). The bedding characters show appears to indicate a sedimentary deposit. Surrounding of the hematite zone was observed barite vein, magnetic anomaly due to magnetite grains. The banding or layer growth nature of hematite is generally considered to be the evidence of the fluid contribution (hydrothermal activity). So, the hematite ore zone was related to hydrothermal activity by the later stage of structural control. According to drilling results, the upper part was covered reddish color clay with iron fragments as well as Fe ores were hosted by clay layers. However, the Fe ore zone

was overlayed the limestone unit. The periphery of the iron ore zones was bounded by carbonate sequences (Silurian limestone and Permian limestone) with sharp contacts. Therefore, the results of the field survey suggest that the Fe enrichment in the overall ore zones occurred concordantly with sedimentation processes whereas mineralization of hematite ores was likely caused by later tectonic events.

CHAPTER 3: Mineralogical and Geochemical study on iron ore and host rocks

3.1. Introduction

The mineralogical and geochemical study may provide valuable information on ore genesis, formation conditions, or serve as indicators in mineral exploration. Mineralogical and geochemical analyses were carried out to understand the details of the origin of mineralization in which geological processes control their distribution. The study was investigated with optical microscopy, X-ray powder diffraction (XRD), X-ray fluorescence (XRF) for the Fe ore samples, and host rocks, as well as acid digestion samples analyzed by ICP-mass spectrometry, stable isotope analysis for Fe ores, fluid inclusion analysis for barite sample.

3.2. Material and methods

3.2.1. Collected samples

Representative ore samples in Pinpet ion deposits were taken from hematite ore zones (H1-H2), limonite ore zones (L1-L9), and magnetic ore samples (Mt11, 23, 25) (Fig. 3.1) as well as host rock samples such as limestone and shale. Topographic maps, aerial photographs, Landsat (satellite) data were studied to obtain the geological features and enhance the previous geological data to understand the reconnaissance geological setting of the study area. Global Positioning System (GPS) was used in collecting representative samples at each target location where lithologic units are well exposed due to erosion, folding, and faulting.

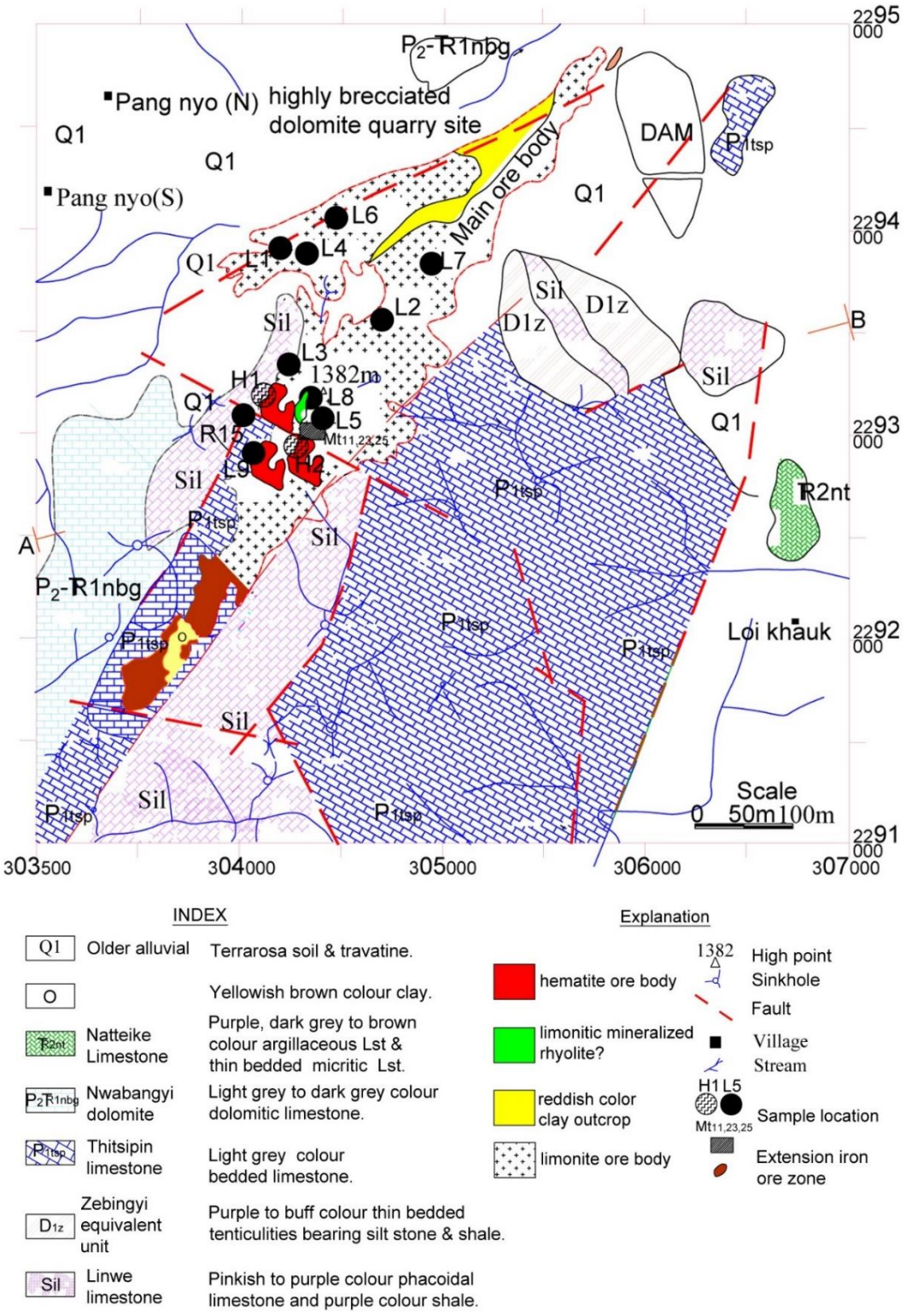

Fig 3.1. Sample location and geological map of the Pinpet iron deposit area (modified after DGSE, 2015).

3.2.2. Analytical methods

Solid samples (hematite, limonite, and magnetic ores) and host rocks were dried at room temperature and pulverized using a Multi-Beads Shocker (PV1001(S), Yasui Kikai) and sieved through a 53 μm stainless steel sieve. The representative powder samples were ignited at 1000º C under 24 hours. After that, a mixture of power samples 0.4 g and 4 g of lithium tetraborate were placed in a platinum crucible for heating at 1000º C for about 8 minutes in TK-4100 bead sampler to get the cooled glass-bead samples. Bulk chemical compositions were determined using glass-bead X-ray fluorescence (XRF; MagiX PRO, Spectris) at the Faculty of Science, Hokkaido University. The X-ray diffractometer (XRD) analyzed using an X-ray diffractometer (Multiflex, Rigaku) equipped with graphite monochromatic CuKα radiation at 40 kV and 30 mA at the laboratory of Nano-micro Material Analysis, Hokkaido University, Sapporo. Samples were scanned from 5°2θ to 70°2θ at a scan speed of 0.02°/s. Fine fractions (< 2μm) of the samples were separated by centrifugation at 3000 rpm for 45 min after being dispersed ultrasonically in deionized water. Those fine fractions were prepared preferred orientation to identify clay minerals by mounting them on glass slides at room temperature with and without ethylene glycol treatment at 60°C overnight. The samples were analyzed using XRD (RINT1200, Rigaku) equipped for CuKα radiation at 30 kV and 20 mA and scanned from 2°2θ to 40°2θ at a scan rate of 1.0°/min.

Bulk concentrations of As, Cu, and Zn were determined by total digestion of 0.4 g of each sample by 15 ml of a 3:1 mixture of HNO_3 (ultrapure grade; Kanto Chemicals) and HF (TAMAPURE AA-100, Tama Chemicals) at up to 180°C for 15 min using a microwave assistant digestion system (ETHOS, Milestone), and analyzed by ICP-mass spectrometry (ICP-MS; iCap Qc, Thermo Scientific) after diluting the solutions by a factor of 10,000.

Sequential extraction of As from the solid samples was conducted using a modified method outlined by Javed *et al*. (2013). Arsenic was extracted from solid samples using various acids, such

as sodium acetate, sodium dihydrogen phosphate, ammonium oxalate, Ti-citrate-EDTA-bicarbonate, hydrogen fluorite, nitric acid, and hydrogen peroxide. Sequential extraction was divided into 10 fractions; F1: soluble by distilled water; F2: exchangeable and loosely adsorbed; F3: strongly adsorbed; F4: carbonate bounded; F5: co-precipitated with amorphous Fe, Al, Mn oxyhydroxides; F6: co-precipitated with crystalline Fe, Al, Mn oxyhydroxides; F7: associated with As oxide and silicate clays; F8: co-precipitated with pyrite and amorphous orpiment; F9: associated with organic matter and secondary sulfides; and F10: residual.

The Fe isotopic compositions were measured by multi-collector ICP-MS (MC-ICP-MS; Neptune Plus, Thermo Scientific) at the Research Institute for Humanity and Nature (Kyoto, Japan). Instrument mass bias was corrected using the standard-sample-standard bracketing method (Weyer and Schwieters, 2003). The procedure for sample digestion using HNO_3 and HF acids at up to 180º C for 15 min using a microwave assistant digestion system (ETHOS, Milestone). Solution samples were loaded into the columns with 1 mL of 8 M HCl, and the matrix was removed by 5 mL 8 M HCl and 5 mL of 3 M HCl. Purified Fe eluates were collected with 4 mL of 0.4 M HCl. The purification process was repeated, to improve purity. The reproducibility of the standard during analyses was overall 95% confidence interval reproducibility is ± 0.10 ‰ (2σ).

Fluid inclusions were studied in two selected barite samples that were collected from barite outcrop in the weathered iron zone. The fluid-inclusion micro-thermometric studies were done on double-polished thin sections (thickness ~90 μm) prepared in the Technical Department, Faculty of Science, Hokkaido University. The measurements were performed on a Linkam LK600 heating-freezing stage that was installed on a Nikon Y-IM microscope at the Department of Earth Resources Engineering, Faculty of Engineering, Kyushu University, Japan. The measured parameters included the last ice-melting temperature (Tm_{ice}) and homogenization temperature (Th). Total salinities for NaCl-H_2O fluid inclusions were calculated from the final ice-melting

temperatures using the equation of wt.% NaCl = 1.78 T – 0.0442 T^2 + 0.000557 T^3, where T is a depression of the freezing point in ºC (Bodnar, 1992).

3.3. Results

3.3.1. Whole-rock geochemistry of host rocks (limestone)

The chemical compositions of the host rock (limestone) are shown in Table 3.1. The major calcium oxide content ranges from 77.4 to 87.3 wt. %, while the magnesium oxide content ranges from 0.8 to 1.2 wt.%. The Fe_2O_3 content range is very low (< 2 wt.%). The SiO_2 values ranged from 5 to 13 wt.%. Alumina ranged between 2.4 – 4.7 wt.%.

Table 3.1. Bulk chemical compositions (major elements) of the host rock (limestone) samples.

Sample	Fe_2O_3 wt%	SiO_2 wt%	Al_2O_3 wt%	MnO wt%	MgO wt%	CaO wt%	Na_2O wt%	K_2O wt%	TiO_2 wt%	P_2O_5 wt%	LOI wt%	Total wt%
R-14	1.3	5.80	2.7	0.1	1.2	87.3	0.25	0.81	0.17	0.07	39.56	99.6
R-15	1.1	7.13	2.4	0.2	0.8	86.9	0.29	0.45	0.08	0.07	27.37	99.4
R-16	2.0	13.2	4.7	0.1	1.1	77.4	0.34	1.21	0.22	0.07	36.78	100

Other elements such as TiO_2 and MnO are less than 0.2 wt.%. Bulk chemical compositions indicate that the host rock (limestone) from the study area falls within the high calcium/pure limestone category whose Ca/Mg ratio falls between 39 and 100 (Todd, 1996).

3.3.2. Petrography and mineralogy of host rocks (limestone, shale)

According to XRD analysis, the shale/clay outcrop consists of micaceous clay, quartz, hematite, and manganese oxide (birnessite) (Fig 3.2a). Based on the ethylene glycol treatment, this clay is non-expanding clay (illite/muscovite) (Fig 3.2b). In the limestone samples, calcite is dominated with some other components include quartz and micaceous clay (Fig 3.2c, d).

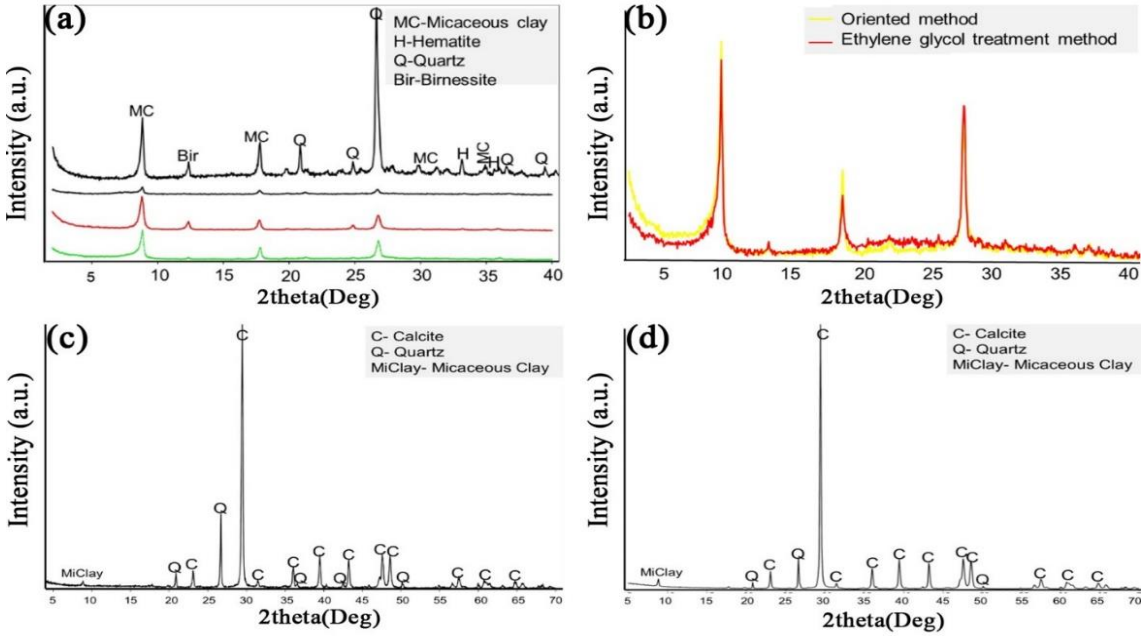

Fig 3.2. X-ray diffraction pattern of clay samples (a), ethylene glycol treatment patterns of clay samples (b), and carbonate host rock (c, d).

Under an optical microscope, limestone is observed to be composed of fine to medium-grained calcite with a minor amount of quartz grains. The oolite textures were also observed under an optical microscope (Fig 3.3a, b). Iron oxide veinlets were observed in the limestone samples (Fig 3.3c, d, e). The other host rock (shale) mainly composed of iron oxide, fine grain detrital quartz (bits), which tend to lie parallel to the foliation (Fig 3.3f).

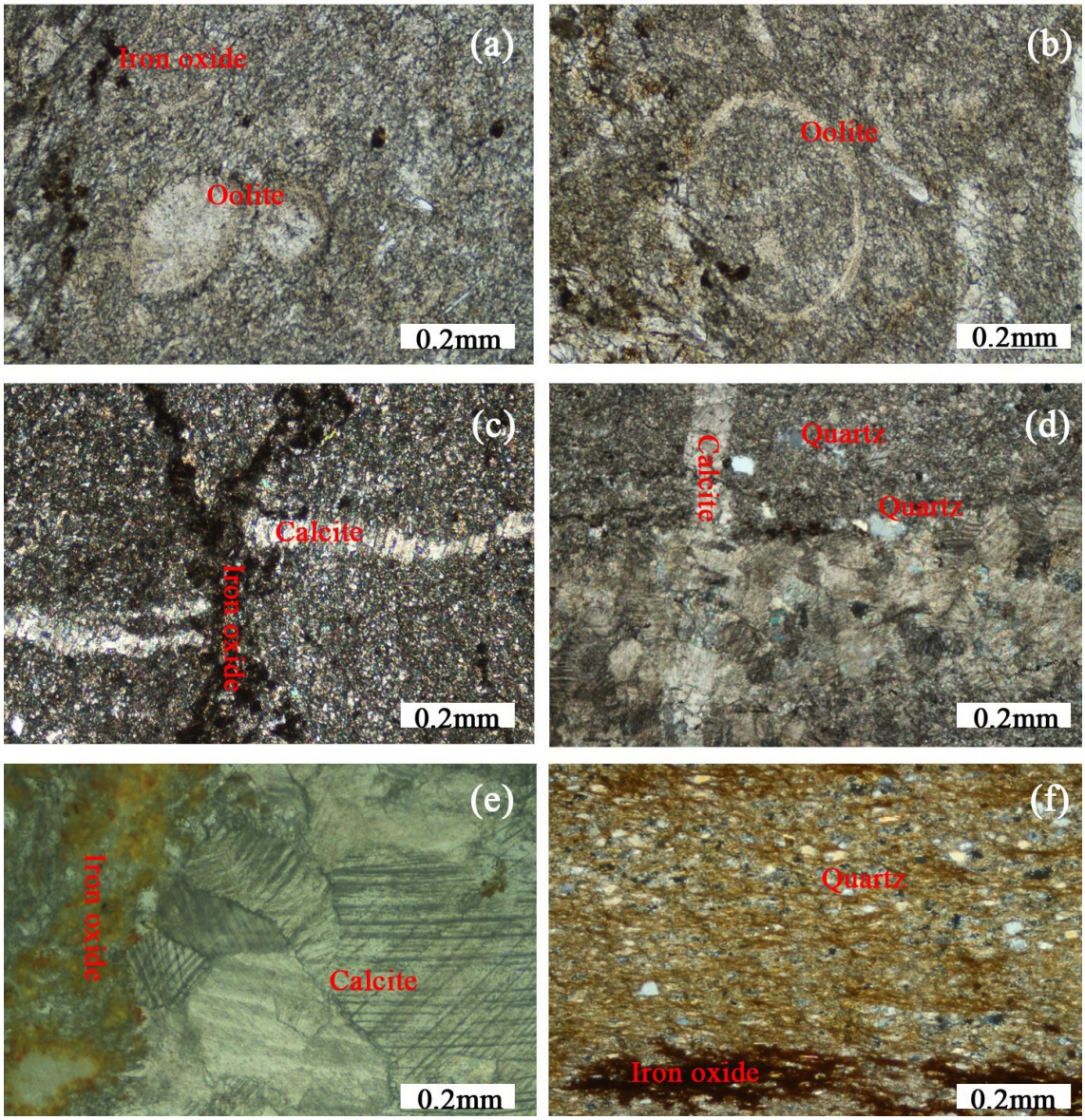

Fig 3.3. Photomicrograph showing of oolite nature in limestone (a, b), quartz grain, calcite, and iron veinlet in Linwe Formation (c, d, e) and quartz grain and iron oxide in shale rock (f).

3.3.3. Whole-rock geochemistry of iron ores

The result of bulk chemical analysis by XRF showed that all the hematite ore samples (H1-H2) and limonite ore samples (L1-L9) are enriched in Fe (61-99 wt.% as Fe_2O_3). Hematite ore samples H1 and H2, in particular, show a high Fe_2O_3 content (99 wt.%) and chemically the hematite ores are almost pure. Other major elements have low wt.% such as SiO_2 (< 0.6), Al_2O_3(<

0.9), CaO (< 0.01). The hematite ore samples showed a low percentage of the loss on ignition (LOI) (~1.2 wt.%). However, LOI percent (11 to 16 wt.%) of limonite ore samples was greater than the hematite ore samples (Table 3.2). Limonite ore samples contained variable amounts of SiO_2 (1 to 12 wt%) and Al_2O_3 (0.4 to 3.0 wt%). Only limonite ore sample L9 contains a significant amount of BaO (8.6 wt.%).

Results of ICP–MS analysis after acid digestion show variable but generally low contents (<1 wt.% or 10000 mg/kg) of hazardous elements in the ores, except for As, which constitutes 2.06 wt.% of sample L1 (Table 3.3). Arsenic contents in the ore samples show highly variable from low (17.8 mg/kg) in sample L4 to high (>1000 mg/kg) in samples L1, L5, and L9 (Fig 3.4). Sample L3 contains relatively high Cu contents (2600 mg/kg), whereas most other ore samples contain 100 to 1000 mg/kg Cu. Zinc concentrations are <100 mg/kg in all of the ore samples. Uranium concentrations in the ores were ~40 mg/kg on average (Table 3.3). Except for limonite samples (L1, L5, and L9), no significant differences in the concentrations of As, Cu, Zn, and U are observed between hematite and limonite ores.

Table 3.2. Bulk chemical compositions (major-elements) of hematite ores (H1 and H2), limonite ore (L1- L9) samples.

Sample	Fe_2O_3 wt.%	SiO_2 wt.%	Al_2O_3 wt.%	MnO wt.%	MgO wt.%	CaO wt.%	Na_2O wt.%	K_2O wt.%	TiO_2 wt.%	P_2O_5 wt.%	BaO wt.%	LOI wt.%	Total wt.%
H1	98.1	0.61	0.90	0.31	0.10	0.01	0.20	0.03	0.06	0.05	B.D	1.31	102
H2	99.2	0.24	0.19	0.24	0.10	0.01	0.20	B.D	B.D	0.03	B.D	1.23	101
L1	76.2	2.44	3.29	0.04	0.25	0.12	0.15	0.33	0.31	0.13	B.D	16.0	99.2
L2	86.7	0.99	1.01	0.04	0.08	0.01	0.33	0.02	B.D	0.02	B.D	12.5	102
L3	79.0	2.88	2.99	0.47	0.11	0.01	0.17	0.16	0.13	0.06	B.D	13.3	99.3
L4	87.3	2.43	0.36	0.33	0.11	0.01	0.19	0.05	B.D	0.06	B.D	11.2	102
L5	73.9	12.2	1.49	0.24	0.14	0.05	0.20	0.29	0.27	0.07	B.D	9.38	98.2
L6	75.2	8.38	3.03	0.08	0.11	0.01	0.19	0.58	0.13	0.03	B.D	12.3	100
L7	68.2	1.88	3.01	0.04	0.46	0.12	0.08	0.27	0.32	0.10	B.D	16.8	91.3
L8	72.9	10.7	1.87	2.22	0.43	0.04	0.18	0.62	0.09	0.03	B.D	11.1	100
L9	60.8	12.5	2.98	0.05	0.19	0.02	0.28	0.48	0.97	0.18	8.62	11.6	98.8

B.D: below the detection limit; LOI: loss on ignition

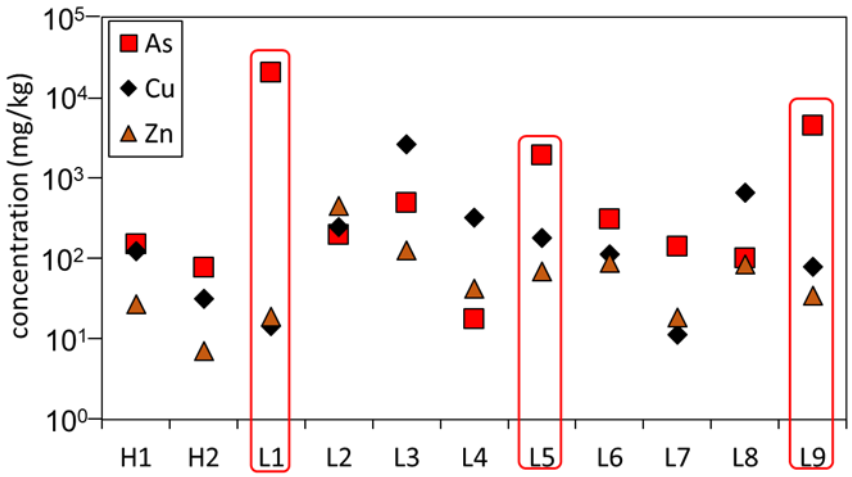

Fig 3.4. Variations in Cu, Zn, and As concentrations in hematite ores (H1 and H2), limonite ores (L1-L9) by acid digestion.

Table 3.3. Bulk chemical compositions (trace-elements) of hematite (H1 and H2), limonite (L1- L9) ore samples.

Sample	Cu mg/kg	Zn mg/kg	As mg/kg	Pb mg/kg	U mg/kg
H1	125	20	152	28	66
H2	32	16	79	7	42
L1	15	24	20700	19	13
L2	246	23	199	454	12
L3	2660	56	497	126	146
L4	328	14	18	43	54
L5	180	18	1940	70	27
L6	113	29	308	90	17
L7	11	12	142	19	12
L8	670	14	101	85	20
L9	79	24	4550	35	16

3.3.4. Petrography and mineralogy of iron ores

The results of XRD analysis showed that hematite is the main ore mineral, with a minor amount of goethite. No accessory minerals in the hematite ore samples were identified by XRD. The limonite ores samples (L1-L9) are dominated by goethite with minor hematite and variable

amounts of quartz. Some limonite ore samples also contain manganese oxides (birnessite; e.g., L3, L6) and barite (e.g., L9), and samples L5 and L8 also contain micaceous clay (Table 3.4; Fig 3.5a), which was identified as non-expanding micaceous clay (illite/muscovite) based on the orientated XRD method with ethylene glycol treatment. Magnetic samples (Mt11, 23, 25) included hematite are dominated followed by goethite, magnetite, gibbsite, and micaceous clay (Fig 3.5b).

Table 3.4. Summary of X-Ray Diffraction analysis on hematite (H1, H2), limonite (L1-L9) ores, and magnetic ore samples (Mt11, 23, 25).

Sample	Hematite	Goethite	Magnetite	Quartz	Barite	Birnessite	Micaceous clay	Gibbsite
H1	+++++	+						
H2	+++++	+						
L1		++++		+				
L2	++	++++						
L3	+	++++				+		
L4		+++++		+				
L5	+	++++		++			+	
L6		++++				++		
L7		+++++		+				
L8		++++		+++			+	
L9	+	++		++	+++			
Mt11	++++	+	++	+				++
Mt23	++++	+++	+	+				
Mt25	+++	++	++	+			+	+

Abundance: +++++ > ++++ > +++ > ++ > +

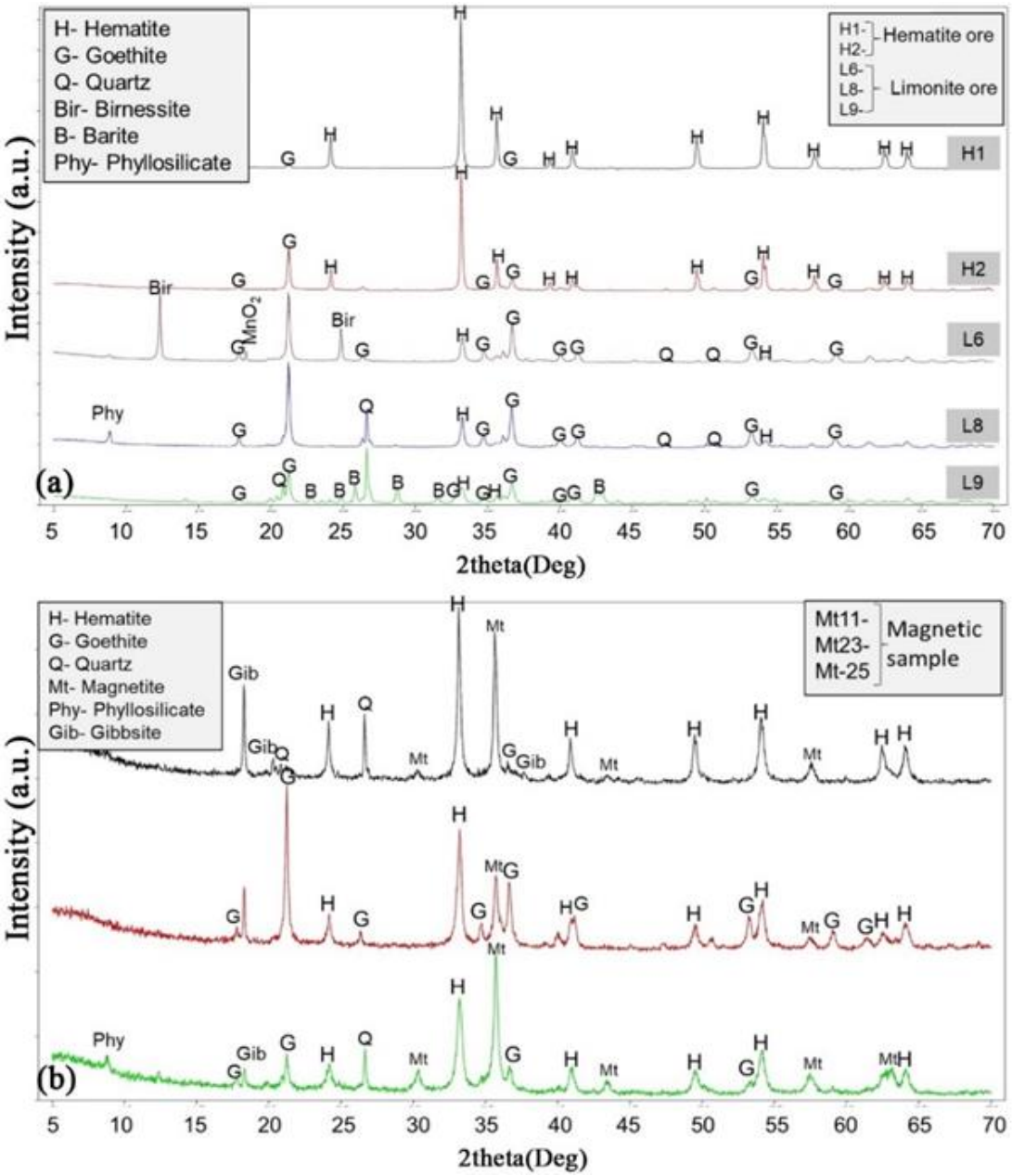

Fig 3.5. X-ray diffraction pattern of hematite and limonite ore (a), and magnetic samples (b). Abbreviations: H-hematite ore sample, L-limonite ore sample, Mt-magnetic sample.

Optical microscope observations reveal that light cream and gray colors hematite mineral was the main component, and some are partly altered to goethite (Fig 3.6a). The limonite samples (L5) consist of euhedral magnetite grain, the light cream color of hematite, and the gray color of goethite (Fig 3.6b). Limonite sample (L-8), that situated not only near the fault zone but also close

to hematite outcrop contained euhedral magnetite grains that are intensely altered to hematite and goethite (Fig 3.6c, d). Furthermore, limonite samples included fine-grain sericite (Fig 3.6e, f). The magnetic samples were altered hematite to goethite (Fig 3.6g). The barite sample contained euhedral lath shape crystals that are abundant (Fig 3.6h).

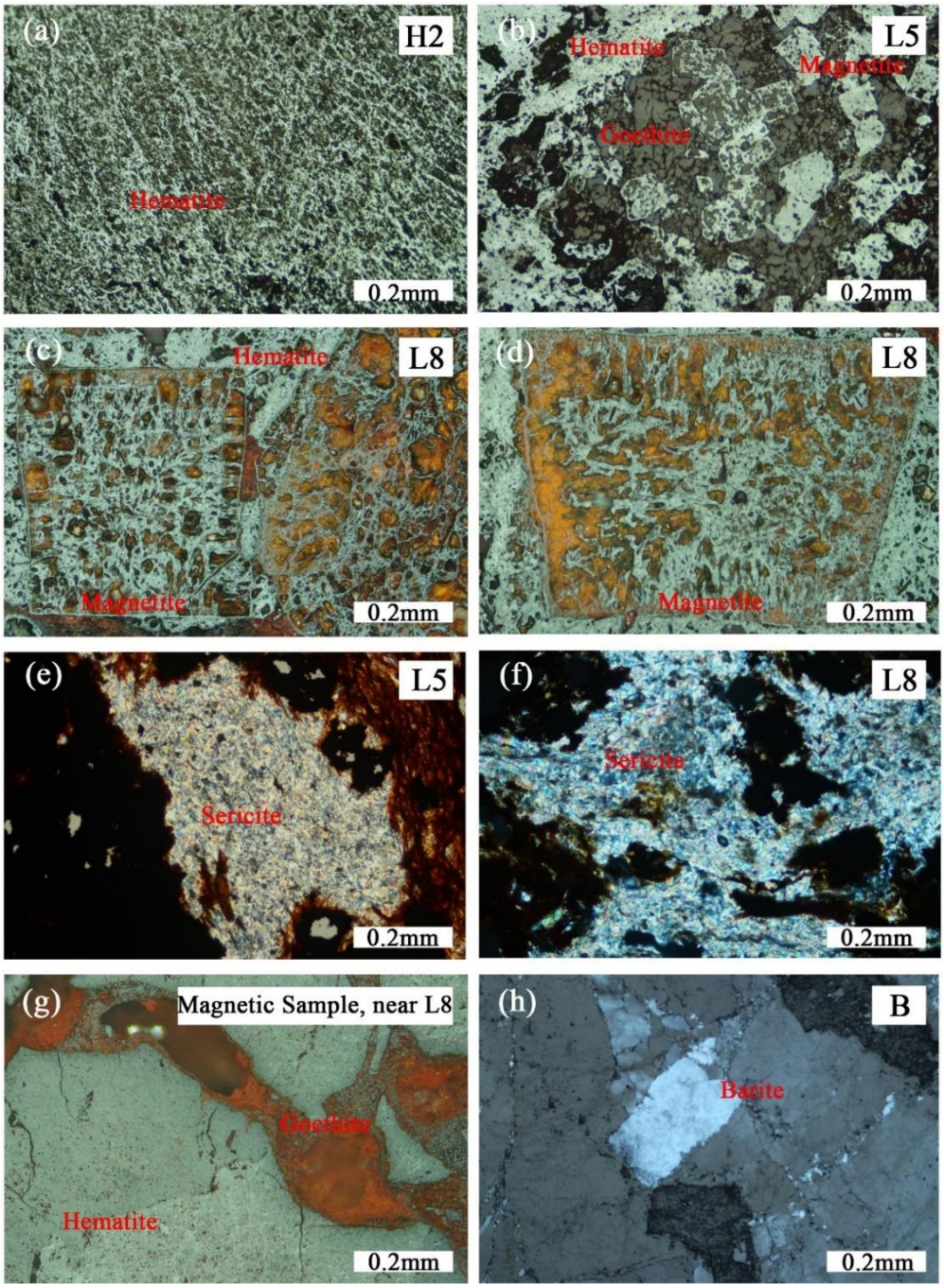

Fig 3.6. Photomicrograph showing (reflected light) of hematite mineral (a), magnetite, hematite, goethite minerals (b), euhedral magnetite minerals (c, d), sericite mineral (e, f), hematite and goethite mineral (g), and barite mineral (h) under transmitted light. Abbreviations: H-hematite ore sample, L-limonite ore sample, B-barite sample.

3.3.5. Sequential extraction of Arsenic in ore samples

The results of sequential extraction for As showing that the following 4 fractions: F6 (co-precipitated with crystalline Fe, Al and Mn hydroxides), F7 (associated with As oxide and silicate clays), F9 (associated with organic matter and recalcitrant sulfides), and F10 (residual) are the dominant phases in both hematite and limonite ores. They occupy more than 90% of the whole As fractions in all the ore samples. Two hematite ore samples (H1, H2) and one limonite ore sample (L4) contain a significant amount of As in the fractions F9 and F10, which are essentially insoluble fractions. Arsenic in other limonite samples were mostly (> 65%) hosted in fractions F6 and F7. In particular, samples L1, L5, and L9, which have a high total As concentration, are dominated by fraction F7 (>50%) followed by fraction F6 (>20%). Labile fractions, F1 (soluble by distilled water), and F2 (exchangeable and loosely adsorbed) fractions were very low (< 0.3%) in all the Fe ore samples (Fig 3.7).

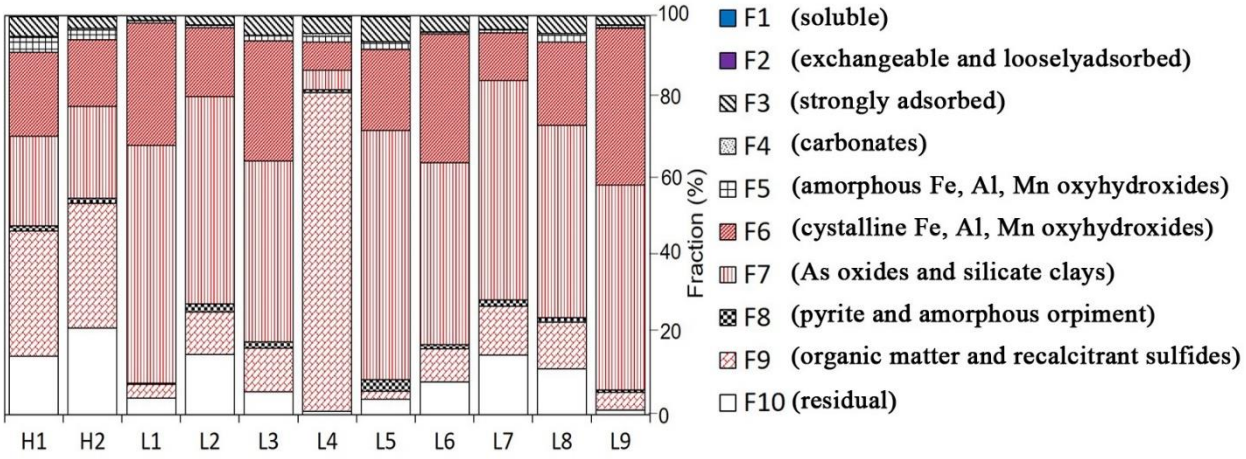

Fig 3.7. Sequential extraction of As from hematite ores (H1, H2) and limonite ores (L1-L9).

3.3.6. Fe isotopes

The stable isotope analysis results for hematite ores (H1, H2) and limonite ores (L1- L10) are listed in Table. 3.5 and illustrated in Fig 3.8. δ^{56} Fe for the hematite ores show a small variation

ranging from – 0.19‰ to – 0.13 ‰. δ^{56} Fe for limonite ores are also variation (except L9: – 1.17 ‰ and L7: + 0.36 ‰) range from – 1.17 ‰ to + 0.36‰.

Table 3.5. Iron isotope composition of hematite (H) and limonite (L) ore samples.

Sample	H1	H2	L1	L2	L3	L4	L5	L6	L7	L8	L9	L10
δ^{56}Fe (‰)	- 0.13	- 0.19	- 0.19	- 0.39	- 0.13	- 0.26	- 0.27	- 0.03	0.36	- 0.24	- 1.17	- 0.18

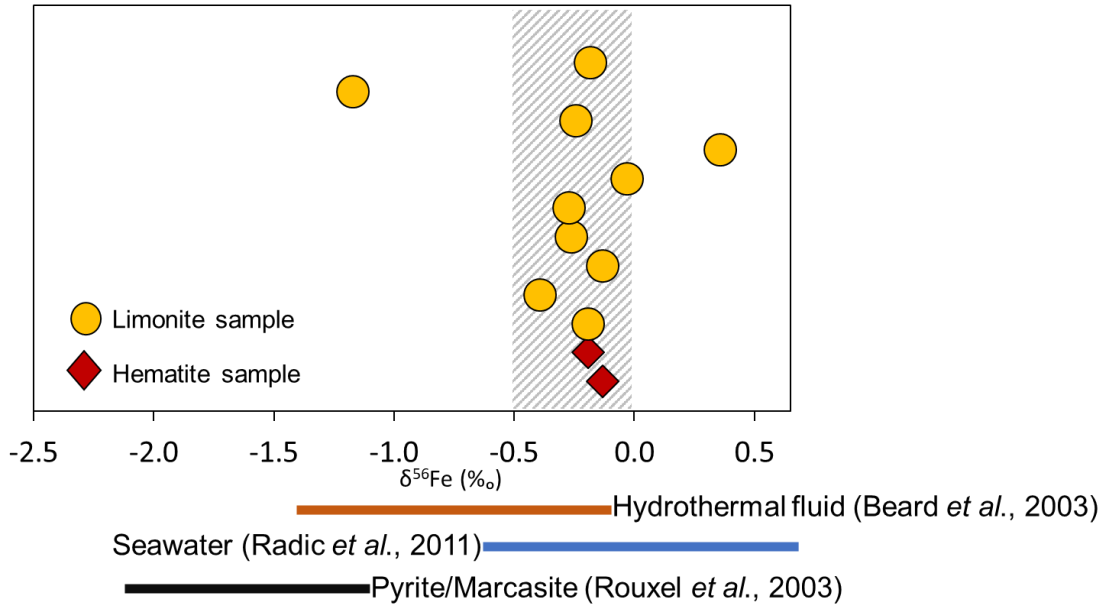

Fig 3.8. Iron isotope compositions of hematite and limonite iron ores.

3.3.7. Fluid inclusions

According to the genetic classification of Roedder (1984), most fluid-inclusion types in barite samples studies are secondary inclusions. The primary and pseudo-secondary inclusions are rarely found in the barite sample. The shape of fluid inclusions is sub-rounded and elongated. The size of fluid inclusions ranges from 2 µm to 8 µm in diameter, majority sizes are 3 µm. They are two-phase (L+V) type recognized in our samples (Fig 3.9). Temperature parameters were measured in two-phase liquid-vapor (liquid-rich) inclusions. The value of homogenization (T_h) temperature measured for more than 30 fluid inclusions of barite samples studied range from 110-190 ºC with an average of 160 ºC (Fig 3.10a). The values of Tm_{ice} varied from – 0.1 ºC to – 4.1 ºC,

the salinity of fluid inclusions (in wt.% NaCl eq.) are salinity ranging from 0.2 to 6.6 wt.%, with peaks at 0.5 and 3.5 wt.% NaCl eq. (Fig 3.10b).

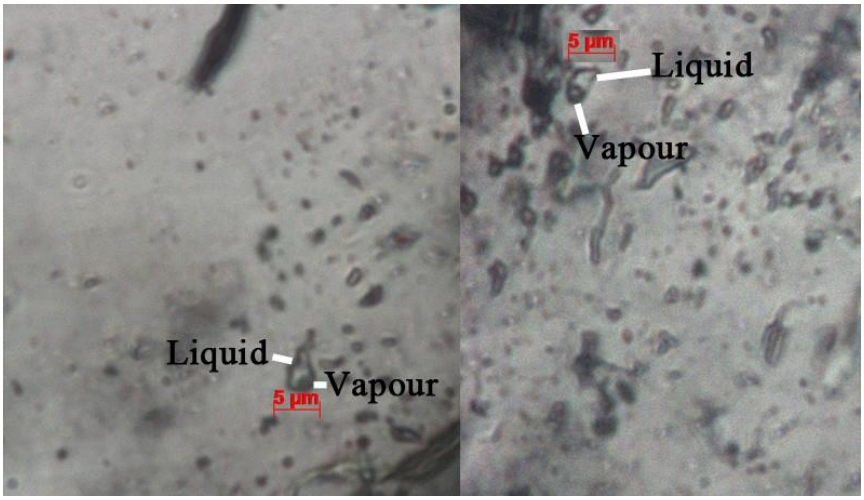

Fig 3.9 Type of fluid inclusions in barite sample.

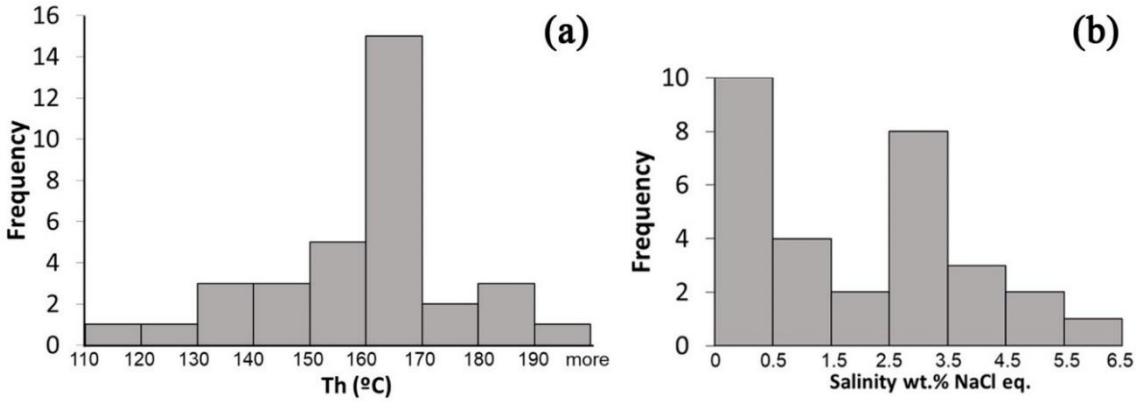

Fig 3.10 Homogenization temperature (a) and salinity of fluid inclusions from barite sample (b).

3.4. Discussion

3.4.1. Mineralogical and geochemical characterization of iron ores

Mineral deposits are heterogeneously dispersed over both space and time, reflecting both the influences of geodynamic setting on mineralization and the transient nature of the specific geological processes that form ores (Goldfarb *et al.*, 2005; Begg *et al.*, 2010; Cawood and Hawkesworth, 2013). Mineralogically, the hematite ores were abundant in hematite mineral which

was partly altered to goethite in the hematite ore. Geochemically the hematite ores have high Fe grade (> 65 wt.%) and low Si content (< 0.28 wt.%), low LOI (~ 1.2 wt.%) and low CaO wt.% (0.01 wt.%). The hematite ore is almost pure and the consisted with low CaO wt.% also the carbonate host rocks contained low Fe wt.% suggested that no relations existed between hematite ore zone and carbonate host rock as well as carbonate host rocks are not the source of iron ore in Pinpet area. Some limonite samples L8 contain euhedral magnetite grains (Fig 3.6c, d) that are altered to hematite and goethite. The limonite samples (L5, L8) consist of sericite (Fig 3.6e, f), manganese oxide (birnessite; L3 and L6), barite in L9. The magnetic sample was altered hematite to goethite (Fig 3.6g). Non-expending micaceous clay (=illite) in clay outcrop also barite vein observed near the hematite zone due to the related hydrothermal activity. According to acid digestion, the method revealed that limonite samples (L1, L5, and L9) with high arsenic concentration (> 1000 mg/kg) that are related to the fault zone. Some limonitic outcrops included magnetite crystals observed in the middle part of the ore zone related to the share-zone near the hematite ore zone.

Under the microscope observation, the euhedral magnetite, sericite observed suggested that related to hydrothermal activities. The limonite samples with high arsenic content due to tectonic activity (e.g., shear or fault intensity and hydrothermal activity). Hydrothermal barite crystals include well-formed polyhedral to euhedral lath-like crystals, often found in radiation bundles or sector-zoned euhedral mineral that project into open vugs (Haymon & Kastener, 1981; Hanor, 2000). In the study area, barite outcrop was observed in the weathered iron zone, which in petrographic observation showed euhedral lath shape crystals are abundant (Fig 3.6h).

Fe isotope technique is probably revealing the origin of the deposit (Jian Sun *et al*., 2013). Iron isotope ratios are partly controlled by hydrothermal fluid circulation (Horn *et al*., 2006; Markel *et al*., 2006). Fe^{2+} rich igneous or metamorphic rocks to insoluble Fe^{3+} weathering products

under oxic conditions occur without significant, production little net change in Fe isotope compositions during the formation of clastic sedimentary rocks, $\delta^{56}Fe$ values is zero. Hydrothermal fluids have an isotope composition significantly different from that of terrestrial igneous ($\delta^{56}Fe \sim 0.0 \pm 0.05‰$) and modern marine sediment ($\delta^{56}Fe \sim + 0.02 \pm 0.07‰$). Direct emanations of Fe^{2+}_{aq} from marine hydrothermal vents have $\delta^{56}Fe \sim – 0.2‰$ to $– 0.5‰$ (Sharma *et al*., 2001, Bread *et al*., 2003a, 2003b).

Isotope analyses of hematite and limonite ores indicate the variable isotope composition ranging from – 1.17 to + 0.36 ‰. The variations in the Fe isotopic signature could be changed in weathering conditions (Manuela A. Fehr *et al*., 2008). Most of the isotope values (except L7 and L9) are within the composition of hydrothermal fluid range (– 0.5 to 0.0 ‰, Beard *et al*., 2003, Severmann *et al*., 2004; Rouxel *et al*., 2008). According to Beard *et al*., 2003, isotope value is relatively low due to a greater amount of hydrothermal input. Ore sample (L9) is a lighter value than other samples could be a greater proportion of hydrothermal input because of ore sample L9 consist of BaO (8.6 wt.%). The stable isotope analysis of Fe in the ores suggested the Fe was precipitated from the hydrothermal fluid in an open system.

The homogenization (T_h) temperature of the barite sample is ranging from 110 - 190 ºC with an average of 160 ºC, the salinity of fluid inclusions (in wt.% NaCl eq.) are ranging from 0.2 to 6.6 wt.%, suggested that the hydrothermal fluid was formed by mixing of seawater with meteoric water.

3.4.2. Alteration of the ore zone

Wall-rock alteration, a common feature of many hydrothermal mineral deposits, and form by the chemical and thermal interaction of hydrothermal fluids or magmas surrounding wall-rock. In the study area, wall rock alterations are not well developed in both sides of host rocks and Fe

ore zone. Sericite was found in the limonite ore samples, in the middle part of the Fe ore zone and also close to the hematite ore zone. Non-expansion clay (illite) was also found in the clay outcrop that related to the shear zone. Sericitization occurred in the iron ore that related to the shear zone. Brecciated quartz was found in the cavity of the limonitic ore zone. Silicification is rarely found in siltstone, shale, and iron ore at the outer part of the iron ore body.

3.4.3. Formation processes of Fe ores

The limonite ore zone is the major portion of the deposit and the hematite ore zone is the second most abundance of total iron ores zones in the Pinpet iron deposit. Limonite occurs as irregular, massive, and poorly bedded nature (Fig 2.8a) with porous texture and iron rose (Fig 2.8c, d) that are of secondary origin due to the weathering process. In several places, limonite is highly weathered and transform in the limonitic soil. The upper part or near-surface of the deposit is characterized by gossan or iron cap exposure due to the leaching process.

The iron ore zone of Pinpet deposit is commonly found adjacent to the carbonate sedimentary sequence (e.g., Silurian age limestone), the sedimentary character of bedding trends is similar to iron outcrop bedding trend although sharp contact with country rock and Fe zone. Surrounding of the hematite ore zone was observed low-temperature hydrothermal activity indicate barite vein, non-expending clay (illite) bearing clay outcrop, magnetite grain, and magnetic anomaly. The shearing effect is most probably due to tectonic movement as indicated by the presence of the polished surface. The shearing effected was changed goethite to the hematite according to the dehydration process equation (1) and (2).

$$2FeOOH.\ nH_2O \longrightarrow Fe_2O_3 + (n+1)\ H_2O \quad (1)$$

$$FeOOH \longrightarrow Fe_2O_3 + H_2O\uparrow \quad (2)$$

Sericitization occurred in the iron ore due to the iron zone related to the shear zone and hydrothermal activity. According to the tectonic, the host rocks block and ore zone might be downthrow or uplift. The actual contact of the host rocks and ore zone area does not show any iron mineralization in the carbonate host rock. Therefore, the Pinpet Fe ore zone was formed as a possible sedimentary process related to hydrothermal activity.

The Fe ore has been mined from different types of ore deposits, including skarn deposits, banded iron formations (BIFs), iron oxide copper-gold (IOCG) deposits, and sedimentary-exhalative (SEDEX) deposits. Most skarns are associated with Fe rich plutons that intruded limestone and volcanic wall rock and form along with the contact. Many deposits are very large (> 500 million ton, > 300 million tons containing Fe) and consist dominantly of magnetite with only minor silicate gangue (Meinert, L. D, 1992). Garnet and pyroxene composition are indicators for the classification of skarn deposits (Einaudi M. T & Burt D. M, 1982; Meinert, L. D, 1993). In the study area, sedimentary carbonate rocks are present, but these rocks are pure limestone, and could not be observed near igneous intrusions. Under the microscopic observation could not observe the skarn mineral (e.g. garnet, wollastonite), suggesting that the Pinpet iron deposit is not a skarn type Fe deposit.

Banded iron formations (BIFs) are chemical sedimentary rocks characterized by alternating silica- and iron-rich bands (Beukes and Klein, 1990; Bekker *et al*., 2010; Li, 2014). The least metamorphosed BIFs commonly consist of chert, magnetite, hematite, carbonates (siderite, dolomite-ankerite), greenalite, stilpnomelane, and riebeckite (Bekker *et al*., 2014). Further, a distinction between the volcanically associated Algoma-type and clastic facies (granular iron formation or GIF) is Superior type sedimentary Lake Superior-type BIFs is made on the basis of the depositional environment (Gross, 1983). These facies support the deep-marine hydrothermal source of iron in BIF (Simonson, 1985a, 2003; Jacobsen & Pimentel-Klose, 1988; Derry &

Jacobsen, 1990; Alibert & McCulloch, 1993). The general belief is that BIFs were formed in a deep-water marine environment. According to the stable isotope analysis of Fe in the ores indicates that the Pinpet ore zone formed Fe was precipitated from hydrothermal fluid in an open system, with no chert layer and alternating silica and iron-rich bands both in the field and microscopic studies, hence the Pinpet iron deposit might not be associated with the BIF deposit.

Iron oxide-copper-gold (IOCG) deposits typically occur at the margins of large igneous bodies which intrude into sedimentary strata. IOCG deposits comprise a wide spectrum of mineralization styles and contain hydrothermal low-Ti Fe oxides (either magnetite or hematite) and Cu-sulfide as major components (Hitzman *et al*., 1992; Hitzman, 2000; Sillitoe, 2003). The common feature of IOCG deposits is alkali alteration and high REE, P, Cu, Au, F, and U content (Williams *et al*., 2005). These ore bodies tend to express as cone-like, blanket-like breccia sheets within granitic margins or massive iron oxides deposits within faults or shears. The genesis of IOCGs is within a magmatic-driven crustal-scale hydrothermal system. The majority of IOCG deposits are recognized to be within Neoproterozoic to the Mesoproterozoic basement. Worldwide, ages of recognized IOCG deposits range from 1.8 Ga to 15 Ma, however, the majority are within the 1.6 Ga to 850 Ma range. The Pinpet iron deposit is a lens shape ore body like a sedimentary layer formed hosted in the Silurian age carbonate sequence. Sulfide minerals (such as pyrite, arsenopyrite as well as copper) could not be observed under mineralogy and geochemical analysis. Ba value in the limonite sample (L-9) is high (8.62%). High Ba content supports hydrothermal type mineralization, but only L-9 location has high Ba value in the study area. The Ba content in hydrothermal solution is much higher than in seawater since affected by sedimentary and volcanic activities (Monnin *et al*, 2001). Pinet iron deposit was formed sedimentation process, could not observe igneous bodies at the surrounding of study. Uranium concentrations in the ores were ~40 mg/kg on average, (except, 146 mg/kg @ L3) in the Pinpet iron deposit. The average concentration

value is 10 times lesser than the Olympic Dam IOCG deposit (Hitzman & Valenta, 2005). Hence, the Pinpet iron deposit could not be associated with the IOCG type.

SEDEX mineralization spans a broad portion of geologic time ranging from ca. 1800 Ma to possible analog forming today. However, peak abundances are well expressed during discrete intervals of the mid-Proterozoic to Paleozoic (600-300 Ma) (Goodfellow *et al*., 1993; Lydon, 1996). SEDEX deposits form distant from volcanic centers (Robb, 2005), and thus the source of metals are solemnly sediments or basement rocks. SEDEX deposits are well known for the large amounts of sulfur contain also barite is more common in the Phanerozoic deposits. According to fluid inclusion analysis of barite indicate that a low-temperature hydrothermal fluid with salinity ranging from 0.2 to 6.6 wt. % NaCl eq was responsible for the formation, suggested that the hydrothermal fluid mixing of seawater with meteoric water. The study area of the Pinpet iron ore deposit was like syn-sedimentary formation during the Paleozoic era but lack of the sulfide assemblage due to the low-temperature hydrothermal condition. However, the Pinpet iron deposit was similar to SEDEX deposits hosted in carbonate rocks.

3.5. Conclusions

Some limonite ore samples contain barite (e.g., L9), and samples L5 and L8 also contain micaceous clay, which was identified as non-expanding micaceous clay (illite/muscovite) also contain sericite and euhedral magnetite observed by microscopy. limonite ore sample L9 contains a significant amount of BaO (8.6 wt%) by XRF analysis. Most of the barite found in the ocean is formed by the mixing of fluids; one containing barium (Ba^{2+}) and another containing sulphate (SO_4^{2-}). Hydrothermal barite precipitates from Ba-rich fluids formed in association with hydrothermal activity ascending from the depth and mixing with seawater near the seafloor. Extensional faults and fractures focus hydrothermal fluids upward onto the seafloor, where they

mix with seawater the primary source of SO_4 for barite precipitation. Barite may also precipitate at intermediate temperature (150 to 250º C) in continental margin hydrothermal settings where fluid circulation driven by high heat flow is common (Hein *et al*., 2007). According to acid digestion, the limonite samples (L1, L5, and L9) which are related to the fault zone area involve high arsenic concentration (> 1000 mg/kg) due to tectonic activity (e.g., shear or fault intensity). Fe isotope values of Fe ores (δ^{56} Fe values between – 1.17 to + 0.36 ‰) suggest that Fe was precipitated from the hydrothermal fluid in an open system. Fluid inclusion analysis showed that a low-temperature (about 160 ºC) hydrothermal fluid with salinity ranging from 0.2 to 6.6 wt.% eq. was responsible for the formation, suggest the hydrothermal fluid was formed by mixing of seawater with meteoric water. Surrounding of hematite ore zone was observed euhedral magnetite grains and sericite bearing iron zone, illite bearing clay outcrop, barite outcrop as well as As-rich limonite ores that are along with minor cross-fault. The results suggest that mineralization of hematite ores and addition of As into the limonite ores occurred during later tectonic activities. Therefore, the Pinpet Fe deposit was related to multiple hydrothermal activities.

CHAPTER 4: Geochemical characteristic of surface water and sediment samples for environmental risk assessment

4.1. Introduction

Water is necessary resources, essential to human life, and health of the environment. As a valuable natural resource, it comprises marine, estuarine, freshwater (river and lake), and groundwater. It is required for most human activities like- drinking, cooking, bathing, washing, agriculture, industry, recreation, and fisheries, etc. About 75% of the world's surface area is covered with water. Out of which 97% of the earth's water is in the ocean, not fit for human use due to its high salt content. Remaining 2% is locked in polar ice caps and only 1% is available as freshwater in rivers, lakes, streams reservoirs, and groundwater, suitable for human consumption (Singh and Kamal, 2014). Water quality issues have become a significant concern due to the growth of population, urban expansion, and technological development. Water can be easily contaminated in different ways through unregulated or regulated but not well designed and monitored disposal practices. Among then, mining is one of the major activities causing water pollution and threatens the quality of surface water and groundwater. Water pollution is caused by mining activities carried out nearby due to overburden dumps, surface impoundments, mine water, acid mine drainage, tailing ponds, etc. (Singh *et al*. 2013). Even tailing from the mineral processing plants affect the surface and groundwater quality. River or streams flowing close to the mining area can be contaminated continuously from the point as well as a non-point source. The problem of water quality degradation and its adverse impacts on the availability of potable and irrigation water, soil quality and agricultural productivity, and biodiversity in the area have been attracting increasing attention of people. The physicochemical parameters are very important because they

have a significant effect on water quality. Therefore, for the measurement of water quality, we need to analyses the physical and chemical parameters of water samples.

Various studies have demonstrated that concentrations of metals in river sediments can be sensitive indicators of the overall contamination in the aquatic systems (Bellucci *et al*. 2002). There are two major routes for metals to enter aquatic environments: natural, (i.e., via rock weathering and erosion) and anthropogenic. The anthropogenic source includes a complex combination of urban, industrial, and agricultural activities and sewage disposal (Schueler, 2000; Çevik *et al*. 2009). In most circumstances, the main input of metals into sediments come from mining and industrial plants along with the rivers (Ridgway *et al*. 2003; Sundaray *et al*. 2011). Aquatic sediments can either retain metals or release them into the water column through various processes of remobilization (Pekey, 2006). The determination of metal concentrations in sediments can be a sensitive indicator of the overall contamination in aquatic systems (Bellucci *et al*. 2002) and represents a useful tool for the identification of anthropogenic contamination sources (Bidhendi *et al*. 2007).

Nan-tank-pauk stream is important for mine water and daily use for villagers in the area, which passes through from north to the south direction in the eastern part of the Pinpet mine area. The uppermost part of the stream meanders through the carbonate area and then reaches the middle and lower parts covered by agricultural soil also isolated carbonate hills. Stream and other tributaries are not far from the mining area may cause continuous contamination from the point source as well as the non-point source. If the Nan-tank-pauk stream is not given attention to water quality degradation, it may pose a serious negative impact on the water resources in the near future. The problems of water quality degradation and its adverse impacts on irrigation water and agricultural productivity in the area have been attracting increasing attention of the local

community. The aim of this chapter is to assess the quality of surface water for suitable domestic purpose and agricultural water in the Nan-tank-pauk stream.

4.2. Material and methods

4.2.1. Sampling methods

The water samples were collected from different locations in two seasons, the wet season (during November 2017) and the dry season (during April-May, 2019). Eight water samples (S1-S8) were collected from different locations of upstream and downstream of the Nan-tank-pauk stream including two water samples from two tributaries: one flowing in the residential area of the mining town (TS1) and another flowing in the main ore zone (TS2). Sampling points are shown in figure 4.1. Tributary samples were obtained only during the wet season because tributaries contained no water during the dry season. Sampling locations were selected based on different land-use patterns. The middle part of the Nan-tank-pauk stream is mostly occupied by agricultural land (Fig. 4.2a). The most downstream site S8 ~10 km down to the south from the mine area (Fig. 4.2b). Sediment samples were taken from sites S5 and S8 in the stream beds. A water sample and a sediment sample were also collected from a tailings dam (DM) in the mine area, which stores rainwater that is used for beneficiation. The sediment samples were obtained by shoveling sediments at 0 – 10 cm depth in the stream beds and stored in polyethylene bags.

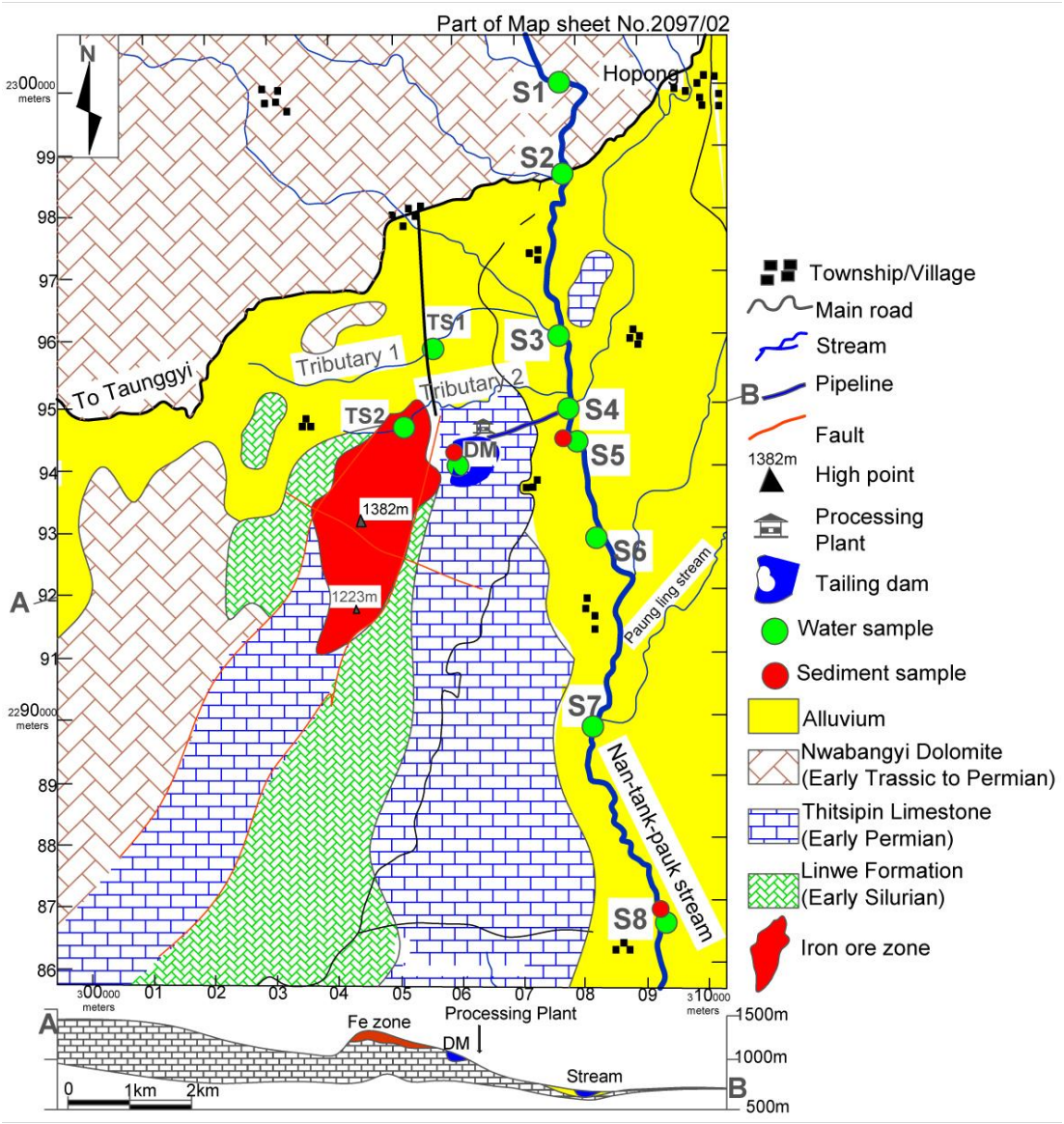

Fig 4.1. Water and sediment samples location map of the study area.

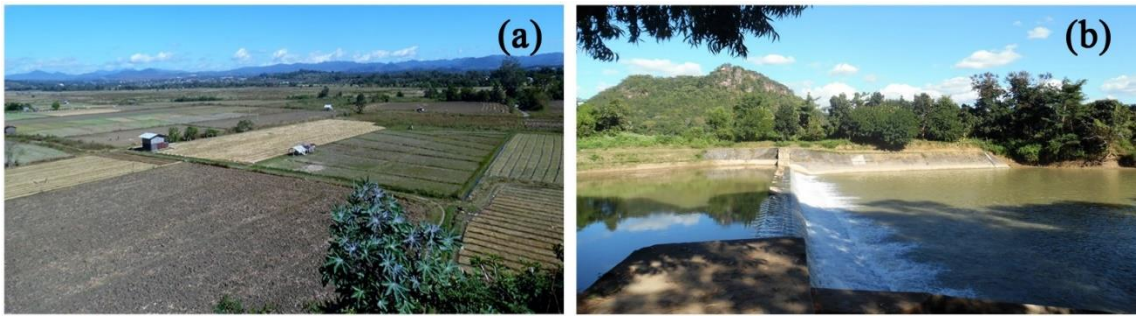

Fig 4.2. Photo showing the agricultural land in the middle part of the Nan-tank-pauk stream (a) and downstream sampling point (b).

4.2.2. Analytical methods

Electrical conductivity (EC), dissolve oxygen (DO), pH, turbidity, temperature, redox potential (Eh), and alkalinity of water samples were measured on-site using (HORIBA, pH/ORP/COND meter D-74). Alkalinity was measured by titrating HNO_3 into the 50ml of a water sample that had been filtered through a 0.45 µm polytetrafluoroethylene (PTFE) membrane filter. The Gran function plot method was applied to obtain the bicarbonate ion (HCO_3^-) concentration from the alkalinity (Rounds, 2015). Water was sampled using a plastic bucket and disposable cups and then filtered using 0.20 µm PTFE membranes in the field. They were completely filled in two 50 ml polypropylene bottles sealed with Teflon tape: one (non-acidified) for anion concentration analysis and the other one (acidified with 1 vol% HNO_3; ultrapure grade, Kanto Chemicals, Tokyo, Japan) for cation concentration analysis. After the samples were transported to Environmental Geology Laboratory, Hokkaido University, they were stored in a refrigerator kept at ~4°C until they were analyzed. Non-acidified samples were diluted 10 times and analyzed for major dissolved anion (SO_4, Cl, and NO_3) concentrations using ion chromatography (861 Advance Compact IC, Metrohm). Acidified water samples were diluted by a factor of 5 and analyzed for major- and trace- metal concentrations measured using inductively coupled plasma-atomic emission spectroscopy (ICP-AES; ICPE-9000, Shimadzu) and ICP-mass spectrometry (ICP-MS; iCap Qc, Thermo Scientific). Standard solutions were prepared using Anion mixture standard solution I (FUJIFILM Wako Pure Chemical), ICP multi-element standard solution IV (Merck), and Indium standard solution (Kanto Chemical).

Sediment samples were dried at room temperature and pulverized using a Multi-Beads Shocker (PV1001(S), Yasui Kikai) and sieved through a 53 µm stainless steel sieve. The sediment samples were ignited at 1000º C under 24 hours. After that, a mixture of power samples 0.4 g and 4 g of lithium tetraborate were placed in a platinum crucible for heating at 1000º C for about 8 min

in TK-4100 bead sampler to get the cooled glass-bead samples. Bulk chemical compositions were determined using glass-bead X-ray fluorescence (XRF; MagiX PRO, Spectris) at the Faculty of Science, Hokkaido University. The X-ray diffractometer (XRD) analyzed using an X-ray diffractometer (Multiflex, Rigaku) equipped with graphite monochromatic CuKα radiation at 40 kV and 30 mA at the laboratory of Nano-micro Material Analysis, Hokkaido University, Sapporo. Samples were scanned from 5°2θ to 70°2θ at a scan speed of 0.02°/s. Fine fractions (< 2μm) of the samples were separated by centrifugation at 3000 rpm for 45 min after being dispersed ultrasonically in deionized water. Sediment samples of preferred orientation were prepared to identify clay minerals by mounting them on glass slides at room temperature with and without ethylene glycol treatment at 60°C overnight. These samples were analyzed using XRD (RINT1200, Rigaku) equipped for CuKα radiation at 30 kV and 20 mA and scanned from 2°2θ to 40°2θ at a scan rate of 1.0°/min.

Bulk concentrations of As, Cu, and Zn in the sediment samples were determined by total digestion of 0.4 g of each sample by 15 ml of a 3:1 mixture of HNO_3 (ultrapure grade; Kanto Chemicals) and HF (TAMAPURE AA-100, Tama Chemicals) at up to 180°C for 15 min using a microwave assistant digestion system (ETHOS, Milestone), and analyzed by ICP-mass spectrometry (ICP-MS; iCap Qc, Thermo Scientific) after diluting the solutions by a factor of 10,000. Previously freeze-dried sediment sample was grounded on agate mortar and dispersed on the specimen mount attached with double tape. Finally, a thin layer of carbon was coated on the sample to allow high electron conductivity during analysis. Samples were analyzed using a Scanning Electron Microscope (SEM) JEOL JSM- IT 200 at the laboratory of Nano-micro Material Analysis, Hokkaido University, Sapporo.

Sequential extraction of As from the solid samples was conducted using a modified method by Javed *et al*. (2013). Arsenic was extracted from sediment samples using various acids, such as

sodium acetate, sodium dihydrogen phosphate, ammonium oxalate, Ti-citrate-EDTA-bicarbonate, hydrogen fluorite, nitric acid, and hydrogen peroxide. The protocols were divided 10 steps (first fraction (F1) to tenth fraction (F10)); F1: soluble by distilled water; F2: exchangeable and loosely adsorbed; F3: strongly adsorbed; F4: carbonate bounded; F5: co-precipitated with amorphous Fe, Al, Mn oxyhydroxides; F6: co-precipitated with crystalline Fe, Al, Mn oxyhydroxides; F7: associated with As oxide and silicate clays; F8: co-precipitated with pyrite and amorphous orpiment; F9: associated with organic matter and secondary sulfides; and F10: residual.

4.3. Result

4.3.1. Physicochemical characteristics of water samples

Water temperature in the Nan-tank-pauk stream ranged from 20.8°C to 22.8°C in the wet season (November) and from 22.6°C to 26.5°C in the dry season (April to May; Table 4.1), which reflects the higher air temperature in the dry season. All the pH values measured during the study were in the neutral to slightly alkaline range in both seasons. The pH gradually increased from 7.3 to 8.2 in the downstream direction in the wet season, which pH at the most downstream site (S8) being higher than that in the dry season (7.9; Table 4.1; Fig. 4.3a). The pH of water in the tailings dam was ~8.5 in both seasons. Eh values were relatively constant at ~450 mV in the wet season but increased gradually from ~360 to ~450 mV in the downstream direction in the dry season (Table 4.1). EC was also constant at 48 – 50 mS/m in the wet season but showed a decrease from 57 to 50 mS/m in the downstream in the dry season (Fig 4.3b). In the west season, turbidity increased markedly from 0.05 FTU at the most upstream site (S1) to 13.1 FTU in the upper and middle reaches of the stream before the entry of tributaries from mine area (S3 and S4) and further increased downstream to 31.8 FTU at S8 (Table 4.1; Fig 4.3c). In the dry season, turbidity was more variable but generally increased in the downstream direction, similar to the pattern observed

for the wet season. The turbidity of tailings dam waters was much higher (28 FTU) in the dry season compared with the wet season (0.3 FTU). Turbidity in both tributaries in the wet season was fairly low (< 10 FTU; Table 4.1). DO values were relatively constant at 7–9 mg/L in the Nan-tank-pauk stream, except for the most upstream (S1) and upper-middle stream (S3) sites, which showed slightly lower DO values of ~6 mg/L in both the wet and dry seasons (Table 4.1).

Table 4.1. Temperature, pH, electrical conductivity (EC), dissolve oxygen (DO), redox potential (Eh), and turbidity of Pinpet water samples. S1-S8: Nan-tank-pauk main-stream; TS1-TS2: tributaries of Nan-tank-pauk steam; DM: tailing dam.

Sample	Temperature °C	pH	EC mS/m	DO mg/l	Eh mV	Turbidity FTU
Nov.,2017 - wet season						
S1	22.1	7.2	49.4	5.88	448	0.05
S2	22.0	7.6	48.9	7.96	473	5.19
S3	22.8	7.5	48.0	6.66	463	13.1
S4	20.8	7.9	46.6	7.98	476	14.1
S5	22.6	8.0	47.6	8.26	428	16.9
S6	22.6	8.1	50.2	8.00	410	20.3
S7	22.3	8.1	48.0	8.27	414	23.1
S8	22.0	8.1	48.0	8.21	431	31.8
DM	23.0	8.4	41.6	9.04	461	0.31
TS1	21.4	8.4	44.7	8.45	475	5.45
TS2	21.4	8.5	55.7	8.35	465	8.07
Apr. to May 2019 - dry season						
S1	23.4	7.2	57	6.62	360	1.83
S2	25.4	7.4	57.1	8.52	357	12.5
S3	24.8	7.5	52.6	5.65	381	5.73
S4	22.6	7.8	54.0	8.64	370	13.8
S5	22.9	7.8	55.0	8.35	365	12.3
S6	25.4	7.9	55.0	8.00	395	11.6
S7	26.5	7.6	49.5	7.36	419	19.4
S8	26.4	7.6	50.0	7.23	447	15.0
DM	26.5	8.7	37.5	8.44	336	28.0
TS1	N.A.	N.A.	N.A.	N.A.	N.A.	N.A.
TS2	N.A.	N.A.	N.A.	N.A.	N.A.	N.A.

N.A.: samples were not available in the dry season

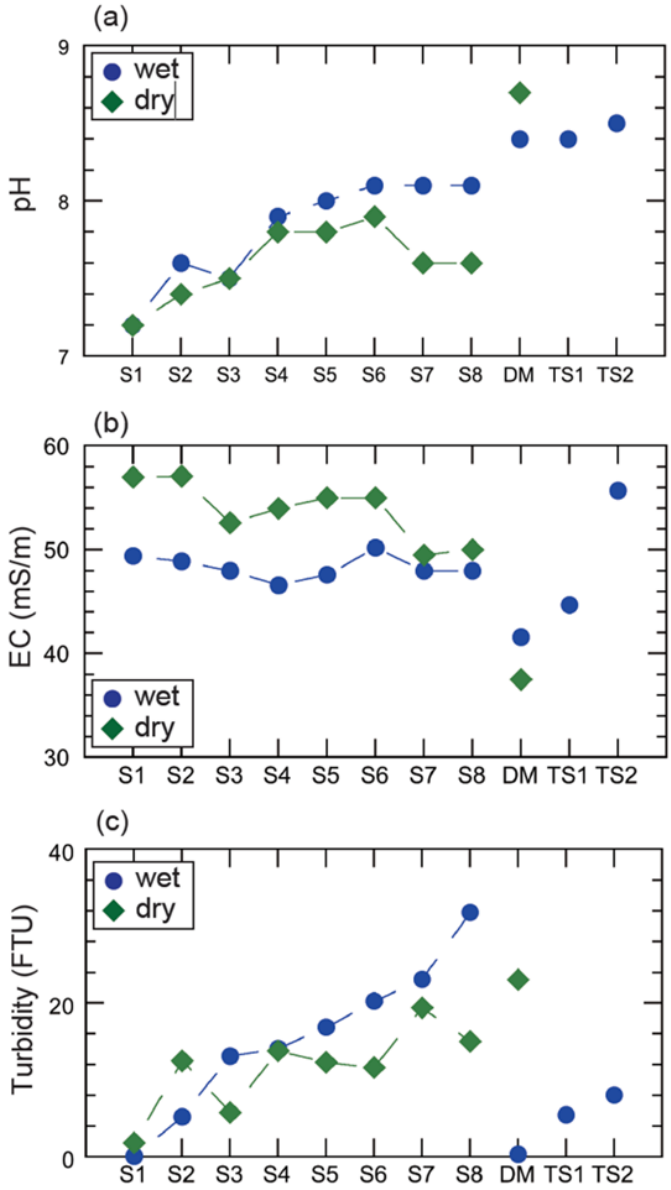

Fig 4.3. Variations in (a) pH, (b) electrical conductivity (EC), and (c) turbidity in the down-stream direction (S1 to S8) in the water of the Nan-tank-pauk stream, and in the tailing dam (DM) and two tributaries (TS1 and TS2), for both the wet (2017) and dry (2019) seasons.

4.3.2. Major and trace elements in water samples

Results of major cation and anion concentration analyses show that all the water samples were dominated by calcium (Ca^{2+}), magnesium (Mg^{2+}), and HCO_3^- (Table 4.2; Fig 4.4). No

significant change in cation or anion concentration was observed in the downstream direction in the Nan-tank-pauk stream (Fig 4.4a and b) or between the wet and dry seasons. Ratios of Mg^{2+} to Ca^{2+} were higher in waters of the tailings dam and the two tributaries compared with the mainstream (Fig 4.4c and d). In the Nan-tank-pauk stream, Ca^{2+} and Mg^{2+} concentrations were fairly uniform, although overall somewhat higher in the wet season (~65 and ~30 mg/L, respectively) than in the dry season (~50 and ~27 mg/L, respectively; Table 4.2; Fig 4.5a). Anions other than HCO_3^- were minor in all the water samples. No significant change in nitrate (NO_3^-) concentration was observed in the downstream direction in the Nan-tank-pauk stream (Fig 4.5b). Although sulfate ions (SO_4^{2-}) were a minor component, their concentrations showed a slight increase downstream from the middle reaches (S4) in the Nan-tank-pauk stream, for example, from ~2 to ~3.5 mg/L in the wet season (Fig 4.5c). SO_4^{2-} concentrations were very low (<4 mg/L) in both the tailings dam and the two tributaries (Table 4.2). Calculated charge imbalance values were within ± 16% for all of the water samples.

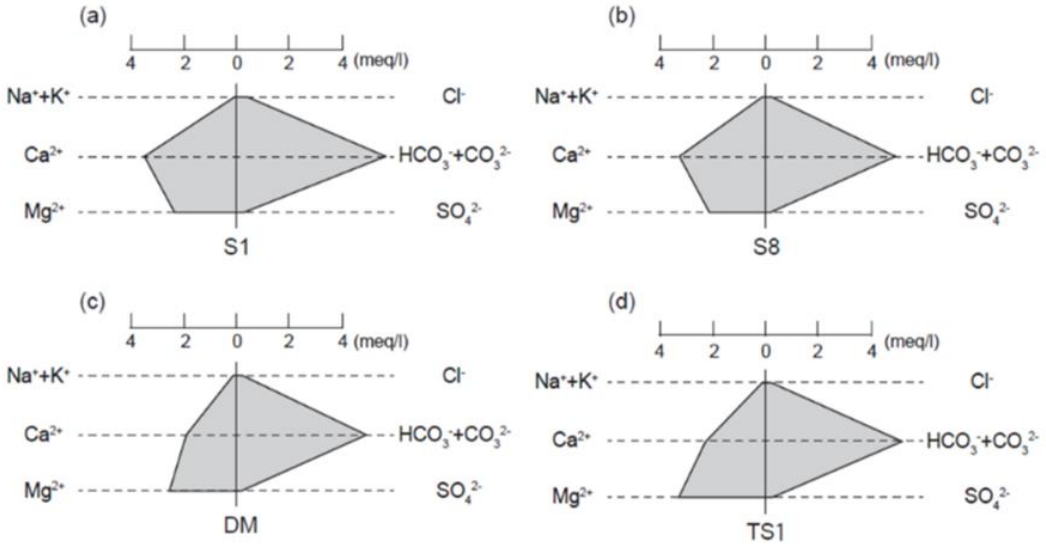

Fig 4.4. Stiff diagrams for water samples from (a) S1 (Nan-tank-pauk stream, most upstream sample), (b) S8 (Nan-tank-pauk stream, most downstream sample), (c) DM (tailings dam), and (d) TS1 (tributary 1) in the wet (2017) season.

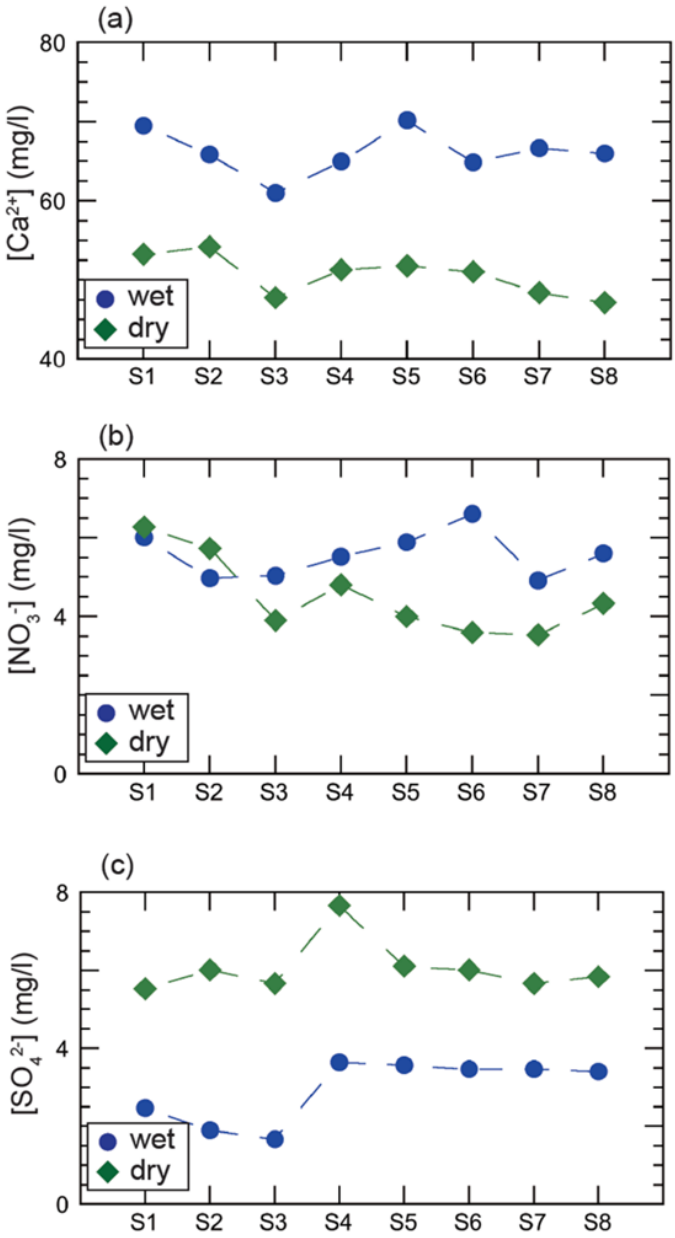

4.5. Variations in (a) Ca^{2+}, (b) NO_3^-, and (c) SO_4^{2-} concentrations in waters of the Nan-tank-pauk stream in the downstream direction (S1 to S8) in the wet (2017) and dry (2019) seasons.

Results of traces elements analyses of water samples show that concentrations of metal and hazardous elements were all lower than 4 µg/L, except for Fe, which was 36.3 µg/L in the tailings dam in the dry season. Other elements detected by ICP-MS analysis include Mn, Fe, Cu, Zn, As, Pb, and U (Table 4.2). Zinc was detectable in the Nan-tank-pauk stream only in the wet season,

and its concentration tended to decrease in the downstream direction (Fig 6a). In the wet season, concentrations of other elements (As, Cu, and Fe) were fairly uniform along the stream even below the mining area. Iron concentrations in the Nan-tank-pauk stream were ~6 to ~11 µg/L. Arsenic, Cu, and Fe concentrations were lower in the tailings dam and the two tributaries than in the Nan-tank-pauk stream. However, during the dry season, their concentrations in the Nan-tank-pauk stream tended to gradually increase in the downstream direction, although the maximum concentrations were <3 µg/L for As and Cu, and <30 µg/L for Fe (Fig 4.6b). Concentrations of these elements were higher in the tailings dam than in the Nan-tank-pauk stream. Uranium was only detectable in the dry season, whose concentrations were ~0.2 µg/L.

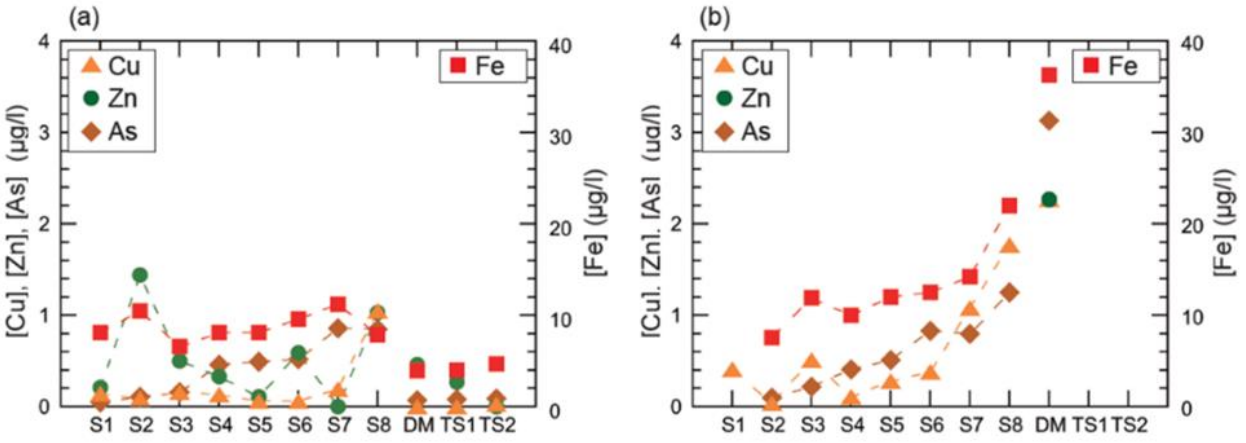

Fig 4.6. Variations in dissolved Cu, Zn, and As concentrations (left axis) and Fe concentration (right axis) in the downstream direction (S1 to S8) in waters of the Nan-tank-pauk stream, and in the tailings dam (DM) and two tributaries (TS1 and TS2), in the (a) wet (2017) and (b) dry (2019) seasons.

Table 4.2. Major cation, anion, and trace-element concentrations in Pinpet water samples and WHO drinking water standards (2004).

sample	Na^+ mg/l	Mg^{2+} mg/l	K^+ mg/l	Ca^{2+} mg/l	HCO_3^- mg/l	NO_3^- mg/l	SO_4^{2-} mg/l	Cl^- mg/l
Nov. 2017 – wet season								
S1	1.02	30.8	0.84	69.5	348	6.01	2.47	0.98
S2	1.13	31.0	1.05	65.9	343	4.98	1.90	0.99
S3	0.94	30.5	1.55	61.0	325	5.04	1.67	0.97
S4	1.50	29.4	0.94	65.0	278	5.52	3.64	1.80
S5	8.54	31.5	4.81	70.2	334	5.89	3.57	1.81
S6	1.34	29.3	0.80	64.9	272	6.60	3.47	1.77
S7	1.51	22.8	1.65	66.7	230	4.92	3.48	1.45
S8	1.30	24.2	0.91	66.0	318	5.61	3.41	1.55
DM	1.20	32.6	1.21	41.1	301	6.12	1.46	1.59
TS1	1.35	39.4	0.80	47.7	339	6.61	1.81	1.84
TS2	1.18	35.8	0.50	60.5	456	4.77	1.47	1.64
Apr. to May 2019 – dry season								
S1	1.19	27.8	0.91	53.3	248	6.27	5.54	1.61
S2	1.23	29.6	1.13	54.2	248	5.73	6.01	1.31
S3	1.14	28.2	1.57	47.8	239	3.91	5.67	1.44
S4	1.46	27.6	0.91	51.3	238	4.81	7.67	2.23
S5	1.45	28.5	1.57	51.8	247	4.00	6.12	2.00
S6	1.50	28.3	0.92	51.1	237	3.59	6.02	2.13
S7	1.58	25.9	1.60	48.4	208	3.54	5.67	1.68
S8	1.43	25.6	0.98	47.2	226	4.33	5.84	1.79
DM	1.19	31.6	1.23	20.5	153	1.95	3.77	2.13
TS1	N.A.	N.A.	N.A.	N.A.	N.A.	N.A.	N.A.	N.A.
TS2	N.A.	N.A.	N.A.	N.A.	N.A.	N.A.	N.A.	N.A.
WHO (2004)	-	-	-	-	-	50	-	-

Sample	Mn µg/l	Fe µg/l	Cu µg/l	Zn µg/l	As µg/l	Pb µg/l	U µg/l
Nov. 2017 – wet season							
S1	0.58	8.11	0.14	0.21	0.05	B.D	B.D
S2	5.62	10.5	0.09	1.44	0.11	B.D	B.D
S3	5.11	6.59	0.16	0.50	0.16	B.D	B.D
S4	8.97	8.10	0.13	0.33	0.46	B.D	B.D
S5	8.61	8.11	0.06	0.11	0.49	B.D	B.D
S6	7.83	9.61	0.06	B.D	0.52	B.D	B.D
S7	6.72	11.2	0.19	B.D	0.86	0.07	B.D
S8	5.52	7.89	1.05	B.D	0.85	0.01	B.D
DM	0.73	3.96	0.10	0.46	0.79	B.D	B.D
TS1	0.82	3.99	0.80	0.27	0.13	B.D	B.D
TS2	1.66	4.68	0.03	B.D	0.32	B.D	B.D
Apr. to May 2019 – dry season							
S1	B.D	B.D	2.41	B.D	B.D	B.D	0.19
S2	65.4	7.55	0.04	B.D	0.10	B.D	0.17
S3	43.5	11.9	0.51	B.D	0.22	B.D	0.17
S4	116	10.0	0.11	B.D	0.41	B.D	0.18
S5	74.9	12.0	0.28	B.D	0.51	B.D	0.18
S6	18.6	12.5	0.38	B.D	0.83	B.D	0.19
S7	5.97	14.2	1.08	B.D	0.80	B.D	0.24
S8	7.27	22.0	1.77	B.D	1.25	B.D	0.24
DM	B.D	36.3	2.27	B.D	3.13	B.D	0.23
TS1	N.A.	N.A.	N.A.	N.A.	N.A.	N.A.	N.A
TS2	N.A.	N.A.	N.A.	N.A.	N.A.	N.A.	N.A
WHO (2004)	400	-	2000	-	10	10	15

N.A.: samples were not available in the dry season
B.D.: below the detection limit

4.3.3 Mineralogical and bulk chemical composition of sediments samples

Results of XRD analysis show that the sediment sample from the tailing dam (DM) is predominantly composed of quartz and calcite, followed by manganese oxide, dolomite, as well as micaceous clay. The mineralogical composition of sample S5, which was taken from the middle reaches of the Nan-tank-pauk stream close to the tailings dam, is similar to that of DM. The most downstream sample (S8) shows a composition to that of sample S5 sample but with more quartz and minor manganese oxide and micaceous clay (Table 4.3). Although Fe (hydr)oxide minerals were not identified (by XRD) in sediments sample (DM), this sample contains ~6 wt% of Fe_2O_3. Results of XRF analysis show that all of the sediments are enriched with SiO_2, (39 – 68 wt.%), S8 sample contained quartz minerals than other sediment samples (DM and S5). All the ore samples were depleted in Na_2O, K_2O, CaO, and MgO (< 1.5 wt% in the total of 4 elements; Table 4.4).

Table 4.3. Summary of X-Ray Diffraction analysis on sediment samples.

Sample	Quartz	Birnessite	Micaceous clay	Calcite	Dolomite
DM	++++	+	++	++	+
S5	++++	+	+	++	+
S8	+++++	+	+		

Abundance: +++++ > ++++ > +++ > ++ > +

Table 4.4. Bulk chemical compositions (major- elements) of sediment samples.

Sample	Fe_2O_3 Wt%	SiO_2 Wt%	Al_2O_3 Wt%	MnO Wt%	MgO Wt%	CaO Wt%	Na_2O Wt%	K_2O Wt%	TiO_2 Wt%	P_2O_5 Wt%	LOI Wt%	Total Wt%
DM	6.20	39.1	12.1	0.11	1.87	7.18	0.19	1.82	0.71	0.09	21.2	90.5
S5	5.47	39.4	14.1	0.15	1.80	10.8	0.19	1.57	0.83	0.14	27.9	102
S8	1.89	68.6	7.41	0.02	0.48	0.35	0.27	1.07	0.67	0.02	5.99	86.7

According to the ethylene glycol treatment, the sediment sample consists of non-expanding micaceous clay (Fig 4.7). SEM analysis shows that an aluminum silicate clay mineral is abundant in both the sediment samples (Figs 4.8a, b, c). This may indicate that the tailing dam sediments (DM) outlet to the nearest sample site (S5) and then downstream site (S8). The Nan-tank-pauk

steam bottom sediments are shown to be related to the tailing dam site through runoff during the wet season.

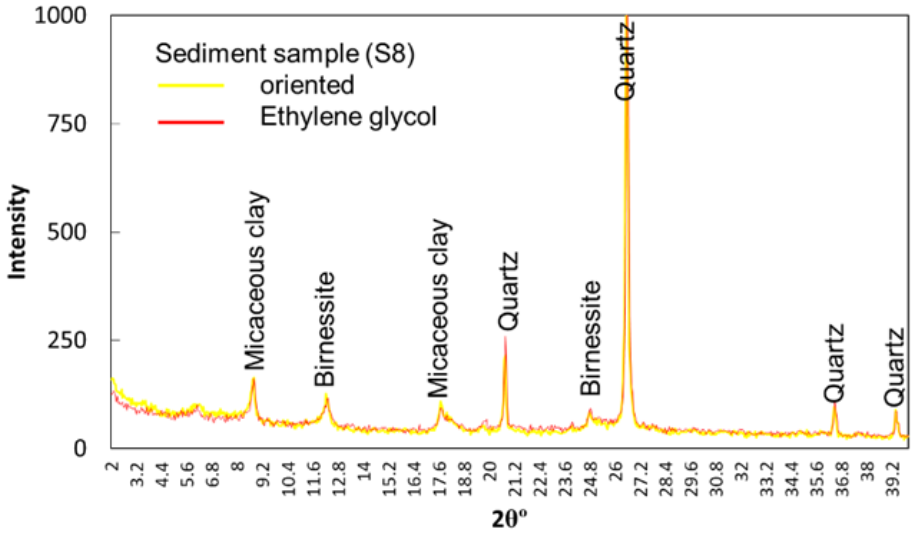

Fig 4.7. Ethylene glycol treatment patterns of clay fraction compositions from sediment samples.

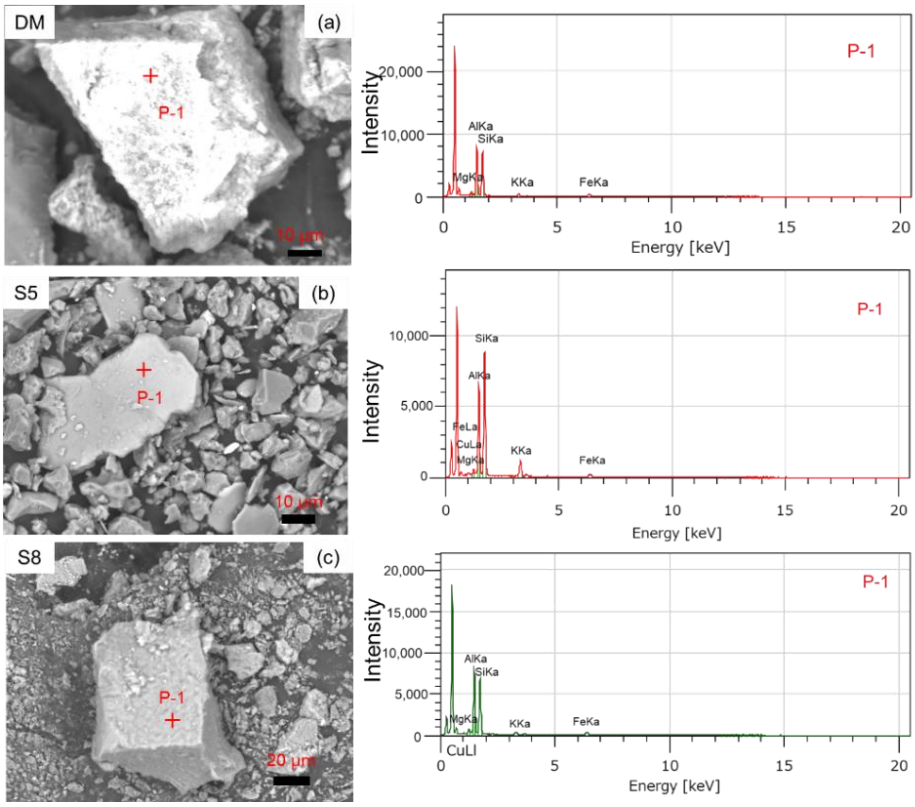

Fig 4.8. SEM photograph of tailing dam (DM) and Nan-tank-pauk stream sediments (S5, S8).

4.3.4. Sequential extraction and acid digestion of As in sediment samples

The results of the sequential extraction of As show that F9 fraction (associated with organic matter and secondary sulfides), and F10 fraction (residual) are the dominant phases in the S8 sample, which has the lowest As concentrations of the sediment samples (Fig. 4.9a). The other two sediment samples (DM and S5) have F6 (co-precipitate with crystalline Fe, Al, and Mn hydroxides) as a significant As-bearing phase in addition to fractions F9 and F10. Metals associated with a residual fraction (F10) are stable and are not soluble under normal environmental conditions. Soluble and exchangeable fractions represent highly bioavailable metals by virtue of metal adsorption when relates to changes in water ionic composition that may affect the adsorption-desorption process and mobility of metals (Fuentes *et al*., 2008). This fraction is of great importance because metals in this fraction can be toxic to aquatic organisms (Davutluoglu *et al*., 2011). But in the study area, labile fractions (F1- soluble by distilled water and F2- exchangeable and loosely adsorbed) fractions were very low (< 0.2%) in all the sediment samples. Result of ICP-MS analysis after acid digestion show no significant difference in the all sediments samples, also low contents of hazardous elements (As, Cu, Zn, U) in the sediment samples from (DM) and Nan-tank-pauk stream (S5 and S8), although arsenic the content of DM is slightly higher (92 mg/kg) than in S5 and S8 (Table 4.5; Fig 4.9b).

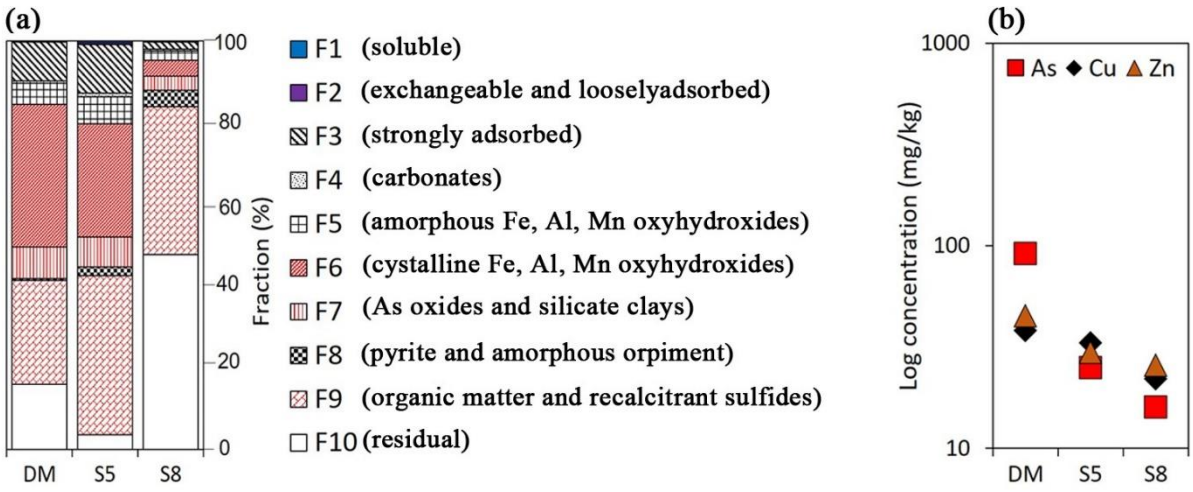

Fig 4.9. Results of sequential extraction and variations in Cu, Zn, and As concentrations in sediment samples (a) ICP-MS analysis after acid digestion (b).

Table 4.5. Bulk chemical compositions (trace- elements) of sediment samples.

Sample	Cu mg/kg	Zn mg/kg	As mg/kg	Pb mg/kg	U mg/kg
DM	38	34	92	45	14
S5	33	37	25	30	13
S8	22	35	16	26	13

4.4. Discussion

4.4.1. Bedrock control on water chemistry and turbidity in Nan-tank-pauk stream

All the pH values measured at the study sites were in the nearly natural to slightly alkaline range in both seasons (Table 4.1), which indicates an absence of the acidic pollution that can be caused by the mining activities such as acid mine drainages (AMD). The dominant cations and anions were Ca^{2+}, Mg^{2+}, and HCO_3^- (Fig 4.4), typical of water in an area with carbonate bedrocks (Appelo & Postma, 2005). The relatively high EC values in the stream water are also consistent with the carbonate bedrock geology (e.g., Ito et al., 2017). The dissolution of carbonate minerals in the bedrocks provides high concentrations of Ca^{2+} and Mg^{2+} (Fig 4.5a), as well as high alkalinity from HCO_3^-. The pH values in the Nan-tank-pauk stream gradually increased in the downstream direction in both the wet and dry seasons (Fig 4.3a), which is likely due to the input of surface

and/or ground waters that had undergone greater reaction with the bedrock downstream or to degassing of CO_2 from the stream water with a high HCO_3^- concentration by aeration via the following reaction:

$$HCO_3^- \rightarrow CO_{2(g)} + OH^- \quad (4.1)$$

The stronger increase in pH in the downstream direction in the wet season suggests a greater influx of water into the lower reaches from the highland region where surface and/or groundwater had reacted with the carbonate bedrocks. Regardless of the along-stream pH gradient, the relatively high pH value indicates that the waters have a buffering capacity, imparting a tolerant to contamination by acidic water in the case that contamination might occur (e.g., Galvez & Sebastien, 1998).

Turbidity also gradually increased in the downstream direction in both wet and dry seasons (Fig 4.3c). The increase in the turbidity was not caused by mining activity because the increase was continuous in the downstream direction and the mining operation is currently suspended. The source of turbidity is likely to have been suspended particulates produced by erosion, agricultural activities on farmland, and dust. The higher turbidity in the wet season compared with the dry season suggests that erosion played an impotent role in the production of turbidity. Turbidity in the tailings dam waters differed substantially between the wet and dry seasons (Fig 4.3c). In the dam, the high turbidity in the dry season reflects a low water level resulting from low precipitation and the consequent sampling depth closer to the bottom.

4.4.2. Present and past anthropogenic influences on stream water and sediment chemistries

Water chemistries measured during this study indicate that mining activity at Pinpet has no influence on the Nan-tank-pauk stream waters. All of the chemical parameters lie within the water quality range specified in the World Health Organization (WHO) standard for drinking water (e.g.,

75 mS/m for EC; WHO, 2004) and the Food and Agriculture Organization standard (e.g., 35 FTU for turbidity; Ayers & Wescot, 1985). All of the measured metal and ion concentrations were also below the WHO standards as well as national quality standards for drinking water proposed by the Ministry of Health and Sports of Myanmar (e.g., 1.0, 0.05, 3.0, and 2.0 mg/L for Fe, As, Zn, and Cu, respectively). In the wet season, no significant external input of metal ions was observed, except for Zn at S2 (Fig 4.6b), which may have been caused by automobile exhausts from the nearby main road (e.g., Akhter & Madany, 1993; Al-Khashman, 2004). Most metal concentrations were higher in the dry than in the wet season and increased in the downstream direction in the Nan-tank-pauk stream. However, the increases were gradual starting from S3 or S4, suggesting that the increase was caused by multiple sources and not a point source such as the mine site. We suggest that the increases in Fe and As concentrations are geogenic and attributable to an increased amount of fine (<0.2 μm) Fe-bearing particulates from eroded materials or dust. Previous studies (e.g., Smedley & Kinniburgh, 2002; Campbell & Nordstrom, 2014) have shown that As is strongly associated with Fe oxides in the natural environment. The coherent behaviors of Fe and As in the Nan-tank-pauk stream suggest that the source and transport processes of these two elements are essentially identical, with As likely being strongly adsorbed onto the surfaces of Fe-oxide particles or incorporated into the crystal structure.

NO_3^- concentrations ranged from 3 to 7 mg/L, which are relatively high values for aquatic plants and animals, particularly in the downstream reaches of the Nan-tank-pauk stream in the wet season, although these values still lie within the WHO environmental standard for drinking water (50 mg/L; WHO, 2004) and the US Environmental Protection Agency (EPA) environmental standard (10 mg/L; US EPA, 2012). The observed values are likely due to increased agricultural runoff in the harvest season (August–September). High concentrations of NO_3^- can cause eutrophication. However, DO values were all well above 5 mg/L (Table 4.1) and at levels suitable

for aquatic life and indicating no or negligible anthropogenic influence. Although SO_4^{2-} concentrations were also low (<8 mg/l), these concentrations showed a slight increase in the middle reaches of the Nan-tank-pauk stream at S3 and S4 (Fig 4.5c) in both the wet and dry seasons, which could be related to mining activity (i.e., the ores are still exposed at the surface), as the change occurred near the mine. The ores are composed of Fe oxides and hydroxides, and although there was no substantial contribution of sulfate ions from the mine site, the slight increase detected may have been caused by impurities in the ores.

As mining activities at Pinpet are currently suspended, it might have been expected that no significant impact on the water chemistry of the Nan-tank-pauk stream would be detected. In contrast, chemical compositions of sediments in the stream could record past anthropogenic influences because hazardous elements in the stream water may be sequestrated and accumulated within sediments. However, bulk chemical compositions of the sediments (Fig 4.10) indicate no such contamination, with As, Zn, and Cu concentrations in the sediments being similar to those in uncontaminated sediments (e.g., Martin & Whitfield, 1983; Kabata-Pendias, 2011). Results of sequential extraction for sediments of sample S5, which is close to the mine site and tailings dam, show that ~50% of As is associated with strongly adsorbed or amorphous or crystalline Fe, Al, and Mn oxyhydroxides (Fig 4.10). The As host phase fraction pattern of S5 is similar to that of sediments from the tailing dam (DM), but different from that of sediments from the most downstream site (S8), which is ~10 km from the mine site. This suggests that a significant proportion of sediments at S5 were transported from the tailings dam, at least for As-bearing minerals. However, this influence was not sufficient to change the bulk chemical compositions of the sediments at S5. Furthermore, because most fractions of As in sediments were found to be insoluble phases, the chemical impacts of sediment-hosted As on the surrounding environment are likely to be minimal.

4.5. Conclusions

This study conducted a geochemical investigation of stream waters in the Nan-tank-pauk stream and its tributaries, which flow through and near the Pinpet Fe mine area in southern Shan State, Myanmar. No significant contamination of surface water caused by mining activity or hematite and limonite ore beneficiation processes was found in the wet or dry seasons. All pH values measured at the study sites are neutral to slightly alkaline. Water alkalinity and Ca^{2+} and Mg^{2+} ion concentrations indicate that the chemical compositions are controlled by carbonate bedrock. All heavy metal and hazardous element concentrations are within the WHO standards for drinking water. Although Fe and As concentrations in the dry season increased in the downstream direction to 36 and 3.1 μg/L, respectively, these increases are inferred to be attributable to a geogenic source, namely the transportation of fine Fe-bearing particulates from eroded materials or dust.

Bulk chemical compositions of sampled sediments in the Nan-tank-pauk stream indicate no significant past contamination by hazardous elements. Arsenic, Zn, and Cu concentrations in the sediments are similar to those in uncontaminated sediments, although some sediments in the tailings dam were probably transported to the middle reaches of the Nan-tank-pauk stream. However, sequential extraction results indicate that most (>90%) of the As in these As-rich ores are hosted in insoluble fractions, probably in the crystal structure of Fe hydroxides and clays. Labile fractions were very low (< 0.2%) in all the sediment samples. Therefore, As is unlikely to be released into the aquatic environment by interacting with water during future ore beneficiation processes should mining be re-established at the Pinpet mine area.

Chapter 5: General conclusions

5.1. Genetic model for Pinpet iron deposit

The Pinpet Fe ore zone was composed of hematite and limonite ores. The Fe ore zone was situated in the carbonate rock sequence especially Silurian age Phacoidal limestone and shale with sharp contacts. The surface of the ore zone has without any overline limestone outcrop. The northern and southernmost of Fe ore zone was pinch out. According to the DGSE drilling results showed the Fe ore was situated above the carbonate rock, occasionally iron ore and clay layer are embedded. The Fe ore zone was dissected by numerous faults striking which are major fault (NE-SE direction) and minor cross fault (WNW-ESE direction). Based on the field observation, in the middle part of the ore zone has the sedimentary nature of well-bedded hematite zones occurred which are deep red colored thin to medium bedded, related to WNW-ESE trending fracture zone and dipping at 40°~ 65° direction (Fig 2.10a) also shear surface was observed (Fig 2.10b). As a result, the surrounding of the hematite zone has a magnetic anomaly, magnetite grains, sericite bearing iron zone, illite bearing clay outcrop, barite outcrop. The predominantly the middle part of the iron zone was affected by a shear effect that formed remineralization of goethite to hematite and follows by these equations.

$$2\alpha\,(FeOOH) \longrightarrow \alpha\,(Fe_2O_3) + H_2O\uparrow \quad (1)$$

$$Fe_2O_3 + Fe^{2+} + H_2O \longrightarrow Fe_3O_4 + 2H^+ \quad (2)$$

According to acid digestion, the limonite samples (L1, L5, and L9) which are related to the fault zone area involve high arsenic concentration (> 1000 mg/kg) due to tectonic activity (e.g., shear or fault intensity). The variations in the Fe isotopic signature could be changed in weathering conditions. Stable isotope analysis of Fe in the ores indicates the variable isotope values (δ^{56} Fe values ranging from – 1.17 to + 0.36 ‰.) almost values are likely to submarine hydrothermal

solution values, suggesting that Fe was precipitated from the hydrothermal fluid in an open system (Fig 5.1a). Fluid inclusion analysis of barite showed that a low-temperature (about 160 ºC) hydrothermal fluid with salinity ranging from 0.2 to 6.6 wt.% eq. was responsible for the formation, suggest the hydrothermal fluid was formed by mixing of seawater with meteoric water. Additionally, the distribution of hematite ores and As-rich ores (L1, L5, L9) are along with the fault trend, suggesting that mineralization of hematite ores and addition of As into the limonite ores occurred during later tectonic activities such as folding and faulting (Fig 5.1b). According to the results, it is concluded that the Pinpet Fe deposit was formed as a result of multiple hydrothermal activities during both sedimentation and faulting events.

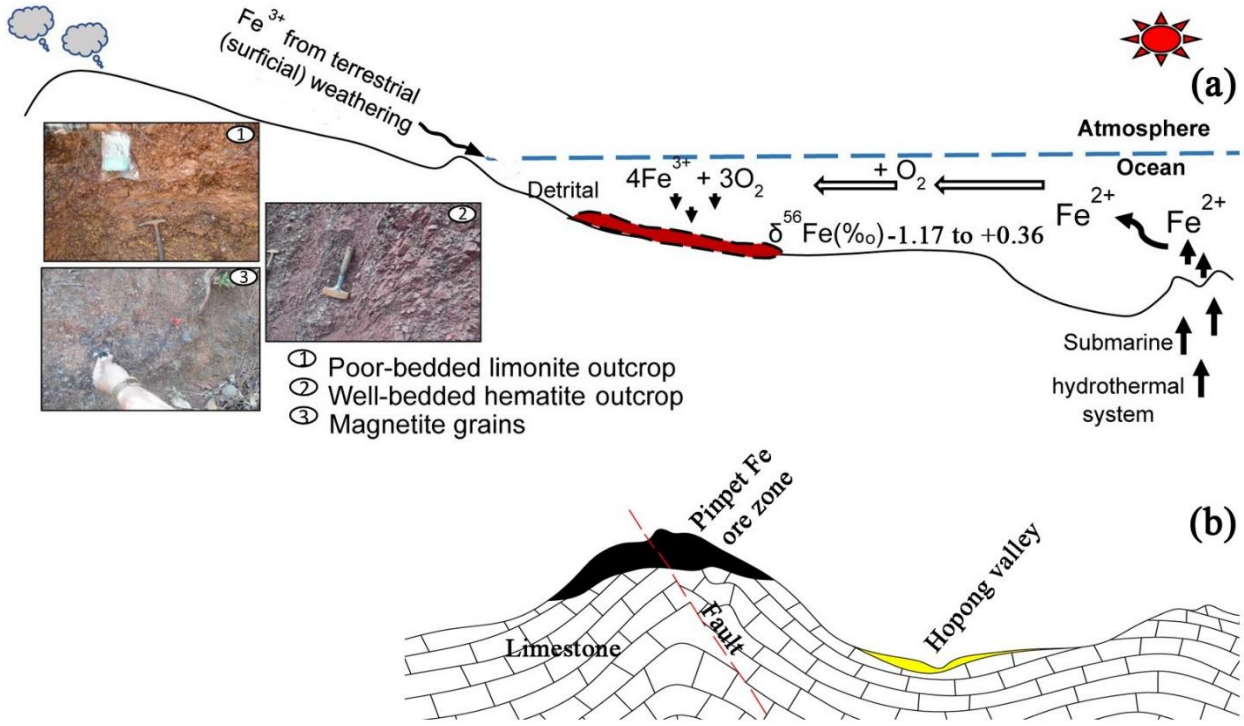

Fig 5.1. Schematic diagram (not to scale) showing the initial formed of Pinpet iron deposit (a) and recent nature of the Pinpet iron zone (b).

5.2. Environmental risk associated with the development of Pinpet mine

Ores in the Pinpet deposit are composed mainly of Fe oxides and hydroxides (i.e., hematite and goethite). Although the origin and formation processes of ores in the Pinpet deposit are poorly understood, significant sulfide mineralization was not detected in our study. Also, no significant concentration of U (> 100 to 1000 mg/kg) was also recognized in the Pinpet deposit (both iron ore and sediments) as found in some IOCG deposits (Hitzman & Valenta, 2005). Exposure of sulfide minerals, particularly pyrite, at the surface by mining activities is known to cause serious environmental issues, such as the occurrence of AMD (Akcil & Koldas, 2006). However, geochemical characteristics of the studied ore samples indicate that there should be no concern regarding AMD in the Pinpet mine, as supported by chemical compositions of water, including pH, and of sediments in the tailings dam.

The primary environmental concern associated with the Pipet deposit is high concentrations of As in some ores (Fig 3.6). Although As concentrations are quite variable in the ore samples, those samples with high concentrations are likely to have undergone enrichment by hydrothermal fluids during activity on WNW–ESE trending faults, which also caused remineralization of goethite to hematite. Therefore, it is possible that a substantial As-rich zone is distributed in the deposit. However, our sequential extraction results indicated that most (>90%) of the As is hosted in insoluble fractions, namely F6 (co-precipitated with crystalline Fe, Al, and Mn hydroxides), F7 (associated with As-oxide and silicate clays), F9 (associated with organic matter and secondary sulfides), and F10 (residual). Together with the results of mineralogical analysis (Table 2), As in samples L1, L5, and L9, which have high total As concentrations, is inferred to be hosted predominantly by Fe hydroxides (i.e., goethite; F6) and clay (i.e., micaceous clay; F7). Because these phases are strongly bound to the minerals (i.e., more tightly than strong adsorption, F3), As is likely to be incorporated into the crystal structure, as commonly observed

in other studies (e.g., Erbs *et al.*, 2010). The metals in exchangeable fractions are considered to be the weakest bonded metals in sediments which may equilibrate with the aqueous phase and thus become more easily bioavailable (Pardo *et al*., 1990). The more proportion of metals in this fraction, the more mobile they are, and the higher the risk they could pose to the environment.

Therefore, it is unlikely that As at Pinpet will be released into the aquatic environment by interacting with water during ore beneficiation such as crushing and magnetic separation conducted in the Pinpet mine. Transportation of very fine particulates through the tailings dam could have delivered Fe and As into sediment of sample S5, which has a higher As concentration than downstream sediment (sample S8). Because As is also hosted in Fe hydroxides, it could be further concentrated during ore beneficiation. Arsenic can be released to the air as a volatile component during smelting. Thus, appropriate treatment of the volatile component will be necessary during smelting should mine operations be restarted.

References

Ahtar Hlaing (2015) Iron exploration of Pinpet extension area. Unpublished DGSE Internal Report [in Myanmar language].

Akcil, A. and Koldas, S. (2006) Acid Mine Drainage (AMD): causes, treatment, and case studies: a review. J. Cleaner Production, 14, 1139-1145.

Akhter, M. S., and Madany, I. M. (1993) Heavy metals in street dust and house dust in Bahrain. Water Air Soil Pollut., 66, 111-119.

Alibert, C. and McCulloch, M. T. (1993) Rare earth element and neodymium isotopic compositions of the banded iron formations and associated shales from Hamersley, Western Australia. Geochim. Cosmochim. Acta, 57, 187-204.

Al-Khashman, O. A. (2004) Heavy metal distribution in the dust, street dust, and soils from the workplace in Karak Industrial Estate, Jordan. Atmos. Environ., 38, 6803-6812.

Appelo, C. and Postma, D. (2005) Geochemistry, Groundwater, and Pollution. CRC Press, Boca Raton, Fl, pp. 668.

Aye Ko Aung (2012) The Palaeozoic stratigraphy of Shan Plateau, Myanmar- an up-dated version. J. Myanmar Geosci. 5, 1-73.

Aye Ko Aung & Cocks, L.R.M. (2017) Cambrian-Devonian stratigraphy of the Shan Plateau, Myanmar (Burma). In: Barber, A.J., Khin Zaw & Crow, M.J. (eds) Myanmar: Geology, Resources, and tectonics. Geological Society, London, Memories, 48, 317-342, https://doi.org/10.1144/M48.14

Ayers, R. S., and Wescot, D. W. (1985) Water Quality for Agriculture. FAO Irrigation and Drainage Paper, 29, Rev.1, Rome, pp. 174.

Beard, B. L., Johnson, C. M., Von Damm, K. L. (2003) Iron isotope constraints on Fe cycling and mass balance in oxygenated Earth oceans. Geology 31:629-632.

Beard, B. L., Johnson, C. M., Skulan, J. L., Nealson, K. H., Cox, L., and Sun, H. (2003a) Application of Fe isotopes to tracing the geochemical and biological cycling of Fe: Chemical Geology, v. 195, p. 87-117.

Begg, G. C., Hronsky, J. A. M., Arndt, N. T., Griffin, W. L., O'Reilly, S. Y., Hayward. N., (2010) Lithospheric, cartonic, and geodynamic setting of Ni-Cu-PGE sulfide deposit. Econ, Geol.105, 1057-1070. https://dx.doi.org/10.2113/econgeo.105.6.1057

Bekker, A., Planavsky, N. J., Krapez, B., Rasmussen, B., Hofmann, A., Slack, J. F., Rouxel, O. J., and Konhauser, K. O. (2014) Iron formation: The origins and implication for ancient seawater chemistry, in Holland, H.D., and Turekian, K.K., eds., Treatise on Geochemistry (2nd ed). Oxford, UK, Elsevier, p. 561-628.

Bekker, A., Slack, J. F., Planavsky, N. J., Krapez, B., Hofmann, A., Konhauser, K. O., and Rouxel, O. J. (2010) Iron formation: The sedimentary product of a complex interplay among metal, tectonic, oceanic, and biospheric processes. Economic Geology and Bulletin of the Society of Economic Geologists, v. 105, p. 467-508. doi:10.2113/gsecongeo. 105.3.467.

Bellucci, L. G., Frignani, M., Paolucci, D., Ravanelli, M. (2002) Distribution of heavy metals in sediments of the Venice lagoon: the role of the industrial area. Sci Total Environ 295:35–49. doi:10.1016/S0048-9697(02)00040-2

Beukes, N. J., and Klein. C. (1990) Geochemistry and sedimentology of a facies transition from micro-banded to the granular iron formation in the early Proterozoic Transvaal Supergroup, South Africa. Precambrian Research, v. 47. P. 99-139, doi:10.1016/0301-9268(90)90033-M.

Bidhendi, N., Karbassi, A., Nasrabad, T., Hoveidi, H. (2007) Influence of copper mine on surface water quality. Int J Environ Sci Technol 4:85–91.

Bodnar. (1993) R.J. Revised equation and table for determining the freezing point depression of H2O-NaCl solutions. Geochim. Cosmochim. 57, 683-684.

Bread, B. L., Johnson, C.M., Von Damm, K. L., and Poulson, R. L. (2003b) Iron isotope constrain on Fe cycling and mass balance in oxygenated Earth oceans: Geology, v. 31, p. 629-632, doi: 10.1130/0091-7613(2003)031<0629:IICOFC>2.0.CO;2.

Campbell, K. M and Nordstrom, D. K. (2014) Arsenic speciation and sorption in a natural environment. A review. Mineral Geochem., 79, 185-216.

Cawood, P. A., Hawkesworth, C. J. (2013) Temporal relations between mineral deposits and global tectonic cycles. Geol. Soc. London. Spec. Publ. 393. https://dx.doi.org/10.1144/sp393.1.

Çevik, F., Göksu, M. Z. L., Derici, O. B., Findik, O. (2009) An assessment of metal pollution in surface sediments of Seyhan dam by using enrichment factor, geo-accumulation index and statistical analyses. Environ Monit Assess 152:309–317.

Cho Cho Myint (1989) Natural Farming in Myanmar, Institute of Agricultural, Pyinmana, Naypyitaw, Myanmar.

Davutluoglu, O. I., Seckin, G., Ersu, C. B., Yilmaz, T., & Sari, B. (2011). Heavy metal content and distribution in surface sediments of the Seyhan River, Turkey. Journal of Environmental Management, 92, 2250–2259.

Derry, L. A., and Jacobsen, S. B. (1990) The chemical evolution of Precambrian seawater: evidence from REEs in banded iron formations. Geochim. Cosmochim. Acta, 54, 2965-2977.

Eckel, C. E. (1902) The preparation of a geologic map. J. Geology, 10-1, 59-66.

Economic and Social Commission for Asia and the Pacific (ESCAP). (1996) Geology and mineral resources of Myanmar. Atlas of mineral resources of the ESCAP Region, United Nations, 12, pp. 74.

Einaudi M. T., Burt D. M. (1982) Introduction, terminology, classification, and composition of skarn deposits. Econ. Geol. and Bulletin of the Society of Economic Geologists, 7, 745-754.

Erbs, J. J., Berquó, S. T, Reinsch, C. V., Lowry, G. V., Banerjee, K. S. and Penn, L. R. (2010) Reductive dissolution of arsenic-bearing ferrihydrite. Geochim. Cosmochim. Acta, 74, 3382-3395.

Fuentes, A., Lloréns, M., Sáez, J., Aguilar, M. I., Ortuño, J. F., & Meseguer, V. F. (2008). Comparative study of six different sludges by sequential speciation of heavy metals. Bioresource Technology, 99, 517–525.

Galvez, C. R., and Sebastien, D. J. (1998) An evaluation of freshwater sediment contamination: the lachine canal sediment case, Montreal, Canada. part II: heavy metal particulate speciation study. Water, Air, Soil Pollut., 102, 281-302.

Goldfarb, R. J., Baker, T., Dube, D., Groves, D. I., Hart, C. J. R, Gosselin, P. (2005) Distribution, character and genesis of gold deposits in metamorphic terranes. In: Hedenquist, J.W., Thompson, J.F.H., Goldfarb, R.J., Richards, J.P. (Eds.), Economic Geology 100th Anniversary Volume, pp. 407-450.

Goodfellow, W. D., Lydon, J. W., Turner, R. J. W. (1993) Geology and genesis of stratiform sediment-hosted (SEDEX) zinc-lead-silver sulphide deposit: Geological Association of Canada Special Paper 40, p. 201-251.

Gross, G. A. (1983) Tectonic systems and the deposition of banded iron formation. Precambrian Res., 20, 171-187.

Hanor, J. S. (2000) Barite-celestine geochemistry and environments of formation. In: Review in Mineralogy & Geochemistry – Sulfate Minerals (Eds C.N. Alpers, J.L. Jambor and D.K. Nordstrom), 40, pp. 193-275. Mineralogical Society of America, Washington, D.C.

Haymon, R. M., and Kastner, M. (1981) Hot-spring deposits on the East Pacific Rise at 21ºN – Preliminary description of mineralogy and genesis. Earth Planet. Sci. Lett., 53,363-381.

Hein, J. R., Zierenberg, R. A., Maynard, J. B. and Hannington, M.D. (2007) Multifarious barite-forming environments along a rifted continental margin, Southern California Borderland. Deep-Sea Res.II, 54.1327-1394.

Hitzman, M. W., Oreskes, N., Einaudi, M. T. (1992) Geological characteristics and tectonic setting of Proterozoic iron oxide (Cu-U-Au-REE) deposits. Precambrian Res 58:241-287.

Hitzman, M. W. (2000) Iron oxide -Cu-Au deposits: what, where, when, and why. In: Proter TM (ed) Hydrothermal iron oxide copper-gold and related deposit: a global perspective. PGC, Adelaide, pp. 9-25.

Hitzman, M. W. and Valenta, R. K. (2005) Uranium in Iron-Oxide-Copper-Gold (IOCG) systems. Econ. Geol., 100, 1657-1661.

Horn, I., von Blanckenburg, F., Schoenberg, R., Steinhoefel, G., Markel, G. (2006). In situ iron isotope ratio determination using UV-femtosecend laser abolition with application to the hydrothermal ore formation process. Geochim Cosmochim Acta 70:3677-3688.

Idriss, A. A., & Ahmad, A. K. (2013). Heavy metals nickel and chromium sediments in the Juru River, Penang, Malaysia. Journal of Environmental Protection, 4, 1245–1250.

Ito, A., Otake, T., Shin, K., Ariffin, K.S., Yeoh, F.Y. and Sato, T. (2017) Geochemical signatures and processes in a stream contaminated by heavy mineral processing near Ipoh City, Malaysia. App Geochem., 82, 89-101.

Jacobsen, S. B., and Pimentel-Klose, M. R. (1988) A Nd isotopic study of the Hamersley and Michipicoten banded iron formations: the source of REE and Fe in Archean oceans. Earth Planet. Sci. Lett., 87, 29-44.

Javed, M. B., Kachanoski, G., and Siddique, T. (2013) A modified sequential extraction method for arsenic fractionation in sediments. Anal. Chim. Acta, 787, 102-110.

Jian Sun, Xiangkun Zhu, Yuelong Chen, Nan Fang. (2013) Iron isotope constraints on the genesis of Bayan Obo ore deposit, Inner Mongolia, China. Precambrian Research 235, 88-106.

Kabata-Pendias, A. (2011) Trace Elements in Soil and Plants, 4th ed. Taylor & Francis Group, Boca Raton, FL, pp. 41-42.

Krupp-Rohstoffe, F. (1962) Iron ore deposit Pinpet: raw material supply, iron, and steel industry Burma. Unpubl. Rep (in German).

Li, Y. L. (2014) Micro and nano-bands in late Archean and Palaeoproterozoic banded iron formations as possible mineral records of annual and diurnal depositions. Earth and Planetary Science Letters, v. 391, p. 160-170. doi:10.1016/espl. 2014.01.044.

Lydon, J. W. (1996) Sedimentary exhalative sulphides (SEDEX), in Eckstrand, O.R., Sinclair, W.D., and Thorpe, R.I., eds., Geology of Canadian mineral deposit types: Geological Survey of Canada, Geology of Canada, v. 8, p. 130-152.

Manuela A. Fehr., Per S. Andersson., Ulf Halenius., Carl-Magnus Morth. (2008) Iron isotope variations in Holocene sediments of the Gotland Deep, Baltic Sea, Geochimica et Cosmochimica Acta 72; p. 807–826

Maung Thein (1973) A preliminary synthesis of the geological evolution of Burma with reference to the tectonic development of Southeast Asia. Geological Society Malaysia, Bulletin, 6, 87-116.

Markel, G., von Blanckenburg, F., Wanger, T. (2006). Iron isotope fraction during hydrothermal ore deposition and alteration. Geochim Cosmochim Acta 70:3011-3030.

Martin, J. M., and Whitfield, M. (1983) The significance of the river input of chemical elements to the ocean. In Wong, C. S., Boyle, E., Bruland, K. W., Burton, J. D. and Goldberg, E. D. (eds.), Trace Metals in Seawater. Plenum Press, New York, pp. 265–296.

Meinert, L. D. (1992) Skarns and skarn deposits. Geosci. Can., 19, 145-162.

Meinert, L. D. (1993) Igneous Petrogenesis and skarn deposits. In. Kirkham R.V., Sinclair W.D., Thorpe R.I., Duke J.M., (Eds.), Mineral Deposit Modeling. Geological Association of Canada, Special Paper, 40, 569-583.

Metcalfe, I. (1996) Pre-Cretaceous evolution of SE Asian terranes. In: Hall, R. & Blundell, D.J. (eds) Tectonic Evolution of Southeast Asia. Geological Society, London, Special Publications, 106, 97-102, https://doi.org/10.1144/GSL.SP.1996.106.01.09

Metcalfe, I. (2009) Late Palaeozoic and Mesozoic Tectonic and Palaeogeographical Evolution of SE Asia. In: Buffetaut, E., Cuny, G., Le Loeuff, J. & Suteethorn, V. (eds) *Late Palaeozoic and Mesozoic Ecosystems in SE Asia*. Geological Society, London, Special Publications, 315, p. 7-23.

Metcalfe, I. (2011) Palaeozoic-Mesozoic History of SE Asia. In: Hall, R., Cottam, M. A. & Wilson, M. E. J. (eds) *The SE Asian Gateway: History and Tectonics of the Australia-Asia Collision.* Geological Society, London, Special Publications, 355, p. 7-35.

Monnin, C., Wheat, C. G., Dupre, B., Elderfield, H., Mottl, M. J. (2001) Barium geochemistry in sediment pore waters and formation waters of the oceanic crust on the eastern flank of the Juan de Fuca Ridge (ODP Leg 168). Geochem Geophys Geosyst 2:1-19.

Pardo, R., Barrado, E., Lourdes, P., Vega, M. (1990) Determination and speciation of heavy metals in sediments of the Pisuerga River. Water Res. 24, 373–379.

Pekey, H. (2006) The distribution and sources of heavy metals in Izmit Bay surface sediments affected by a polluted stream. Mar Pollut Bull 52:1197–1208.

Ram Bahadur Sah and Kabi Raj Paudyal. (2019) Geological control of mineral deposits in Nepal, J. Nepal, Geological Society, vol 58, pp 189-197.

Ridgway, J., Breward, N., Langston, W. J., Lister, R., Rees, J. G., Rowlatt, S. M. (2003) Distinguishing between natural and anthropogenic sources of metals entering the Irish Sea. Appl Geochem 18:283–309.

Robb, L. J. (2005) Introduction to Ore-Forming processes. Blackwell Publishing, Oxford, p. 373.

Roedder, E. (1984) Fluid inclusions. Rev.Miner. 12, 644.

Rounds, S. A. (2015) Alkalinity and acid-neutralizing capacity. In Wilde, F. D. (Ed.), National Field Manual for the Collection of Water-quality Data. Handbooks for Water-Resources Investigations. USGS, Reston, VA.

Rouxel, O., Shanks, W.C., III, Bach, W., and Edwards, K. (2008) Integrated Fe and S isotope study of seafloor hydrothermal vents at East Pacific Rise 9-10 N: Chemical Geology, v. 252, p. 241-227.

Schueler, T. R. (2000) Cars are a leading source of metal loads in California. The Practice of Watershed Protection, Ellicott City.

Severmann S, Johnson CM, Beard BL, German CR, Edmonds HN, Chiba H, Green DRH (2004) The effect of plume processes on the Fe isotope composition of hydrothermally derived Fe in the deep ocean as inferred from the Rainbow vent site, Mid-Atlantic Ridge, 36degree 140 N. Earth Planet Sci Lett 225:63-76.

Sharma, M., Polizzotto, M., and Anbar, A. D. (2001) Iron isotopes in hot springs along the Juan de Fuca Ridge: Earth and Planetary Science Letters, v. 194, p. 39-51.

Sillitoe, R. H. (2003) Iron oxide-copper-gold deposits: an Andean view. Miner Deposita 38:787-821.

Simonson, B. M. (1985a) Sedimentological constraints on the origins of Precambrian iron formations. Geol. Soc. Am. Bull., 96, 244-252.

Simonson, B. M. (2003) Origin and evolution of large Precambrian iron formations. In: Extreme Depositional Environments: Mega-End Members in Geologic Time (Eds M. Chan and A. Archer), Geol. Soc. Am. Spec. Paper, 370, (in press)

Singh, P. K., Tiwari, A. K., and Mahato, M. K. (2013) Qualitative Assessment of Surface Water of West Bokaro Coalfield, Jharkhand by Using Water Quality Index Method International Journal of ChemTech Research, 5(5).

Singh, G., and Kamal, P. K (2014) Application of Water Quality Index for Assessment of Surface Water Quality Status in Goa. Current World Environment, v 9 (3), 994-1000.

Smedley, P. L., and Kinniburgh, D. G. (2002) A review of the source, behavior, and distribution of arsenic in natural waters. Appl Geochem., 17, 517-569.

Soe Min, Soe Thura Tun, Watkinson, I. M., and Win Naing (2016) The Kyaukkyan Fault. In: Barber, A.J. Ridd, M.F., Khin Zaw & Rangin, C. (eds.) Myanmar: Geology, Resources, and tectonic. Geological Society, London, Memoir, 21, 453-472.

Sundaray, S. K., Nayak, B. B., Lin, S., Bhatta, D. (2011) Geochemical speciation and risk assessment of heavy metals in the river estuarine sediments— a case study: Mahanadi basin, India. J Hazard Mater 186:1837–1846.

Todd T. W. (1996) Petrographic classification of carbonate rocks. Journal of Sedimentary Petrology. 36 (2):317-340.

U.S. Environmental Protection Agency (2012) Edition of the Drinking Water Standards and Health Advisories [EPA 822-S-12-001].

Weyer, S., Schwieters, J. (2003) High precision Fe isotope measurements with high mass resolution MC-ICP-MS. Int. J. Mass Spectrom. 226, 355-368.

Williams, P.J., Barton, M.D., Johnson, D.A., Fontbote, L., De Haller. A., Mark, G., Oliver, N.H.S., Marschik, R. (2005) Iron oxide copper-gold deposits: Geology, space-time distribution, and possible modes of origin. Economic Geology 100th anniversary volume: 371-405.

Win Swe & Win Naing (2008) Seismicity and major active faults in Myanmar. Journal of the Myanmar Geosciences Society, 1, 1-20.

World Health Organization (2004) Guidelines for Drinking Water Quality, 3rd ed, Geneva.

Zaw Win, Kyi Kyi Shwe & Ohnmar Soe Yin (2017) Sedimentary facies and biotic associations in the Permian-Triassic Limestone on the Shan Plateau, Myanmar. In: Barber, A.J., Khin Zaw & Crow, M.J. (eds) *Myanmar: Geology, Resources, and tectonics*. Geological Society, London, Memories, 48, 343-363, https://doi.org/10.1144/M48.15